Profound seizure suppression and disease modification by targeting JAK1, a key driver of a pro-epileptogenic gene network.

Olivia R. Hoffman[1,2], Anna M. Patterson[1], Emily S. Gohar[1], Emanuel Coleman[3], Jose Ezekial Clemente Espina[4], Barry A. Schoenike[1], Claudia Espinosa-Garcia[4], Felipe Paredes[5], Raymond J. Dingledine[5], Jamie L. Maguire[3], Avtar S. Roopra[1,2]*

[1]Department of Neuroscience, University of Wisconsin-Madison School of Medicine and Public Health, Madison, WI 53705, USA; [2]Molecular and Cellular Pharmacology Graduate Program, University of Wisconsin-Madison School of Medicine and Public Health, Madison, WI 53705, USA; [3]Department of Neuroscience, Tufts University School of Medicine, Boston, MA 02111, USA; ; [4]Cellular and Molecular Biology Graduate Program, University of Wisconsin-Madison School of Medicine and Public Health, Madison, WI 53705, USA [5]Department of Pharmacology & Chemical Biology, Emory University School of Medicine, Atlanta, GA 30322, USA.

ABSTRACT

Epilepsy is the 4th most prevalent neurological disorder with over 50 million cases worldwide[1,2]. While a number of drugs exist to suppress seizures, approximately 1/3 of patients remain drug resistant, and no current treatments are disease modifying[3]. Using network and systems-based approaches, we find that the histone methylase EZH2 suppresses epileptogenesis and slows disease progression, via repression of JAK1 and STAT3 signaling in hippocampal neurons. Pharmacological inhibition of JAK1 with the orally available, FDA-approved drug CP690550 (Tofacitinib)[4,5] profoundly suppresses behavioral and electrographic seizures after the onset of epilepsy across preclinical rodent models of acquired epilepsy. This seizure suppression persists for weeks after drug withdrawal. Identification of an endogenous protective response to status epilepticus in the form of EZH2 induction has highlighted a critical role for the JAK1 kinase and STAT3 in both the initiation and propagation of epilepsy across preclinical rodent models and human disease. Overall, we find that STAT3 is transiently activated after insult, reactivates with spontaneous seizures, and remains targetable for disease modification in chronic epilepsy.

INTRODUCTION

Epilepsy is a highly prevalent neurological disorder with over 50 million cases worldwide[1,2]. Arising from a myriad of etiologies including gene mutations and environmental insults, the unifying characteristic of the epilepsies is the emergence of recurring, spontaneous seizures. Epileptogenesis is the process that links initial insults to the eventual propagation of spontaneous seizures. One of the insults that may initiate epileptogenesis is status epilepticus: an unremitting bout of seizures lasting for more than five minutes, during which the patient does not regain consciousness[6-8]. The first-line treatments for epilepsy are anticonvulsants aimed at controlling seizures. While these medications effectively suppress seizures for some patients, they do not target the processes that orchestrate progression of the disease, and fail to suppress seizures altogether in approximately 1/3 of patients[3]. There is a critical need for treatments that target the progressive decline in seizure threshold that arguably leads to spontaneous seizures.

A poor understanding of the mechanisms underlying epileptogenesis has so far prevented the development of disease biomarkers and translation of antiepileptogenic treatments from pre-clinical rodent models to the clinic. Although others have reported the disease-modifying potential of manipulations to metabolism[9-11], inflammation[12,13], chromatin modification[14], and signal transduction pathways[15], progress has been hindered by a lack of consensus among laboratories employing different models of status epilepticus (SE)[16]. With few exceptions[9,17-20], little effort has been made to identify the principal transcription factors and chromatin modifiers whose function precipitates the gene changes that arise after status epilepticus.

Recently, we applied a systems approach and novel bioinformatic tool[21] to a transcriptomic consortium dataset that incorporated gene expression data across multiple laboratories and models of epilepsy[22]. This allowed for identification of potential mechanisms that span across rodent models of status epilepticus (SE) and human temporal lobe epilepsy (TLE)[23]. With this approach, we identified the histone methylase Enhancer of Zeste Homolog 2 (EZH2) as a potential driver of gene changes in dentate granule cells post-SE that is induced by an order of magnitude across epilepsy models. Transient pharmacological inhibition of EZH2 post-SE worsened

epileptic phenotypes one month later, suggesting that EZH2 induction plays a protective role in epileptogenesis. In addition to EZH2, our analysis predicted Signal Transducer and Activator of Transcription 3 (STAT3) to be a driver of gene activation across models of SE[22,23].

Of the studies that have profiled gene changes in the epileptic brain, nearly all find a robust activation of inflammatory pathways[17-20,23-25]. In the brain, inflammation can be triggered by glial cells[26], but neurons also exhibit an innate immune response that has been associated with hyper-excitability[27]. Anti-inflammatory drugs have been used with varying degrees of success to suppress seizures in human patients[28-31], and some drugs targeting neuroinflammation in rodents have shown antiepileptogenic potential[32-35]. However, the endogenous mechanisms that regulate neurogenic inflammation post-SE are poorly understood.

Herein, we show that EZH2 induction with SE suppresses pathological activation of pro-inflammatory JAK/STAT signaling in neurons, both in animal models and human disease. EZH2 deletion in neurons leads to hyper-activation of the JAK/STAT pathway, robust reductions in seizure threshold after SE, and an exaggerated epileptic phenotype. Pharmacological inhibition of JAK1/3 activity acutely after SE rescues these phenotypes. Finally, targeting STAT3 reactivation after the onset of epilepsy with the JAK inhibitor CP690550 results in an enduring, disease-modifying suppression of spontaneous seizures.

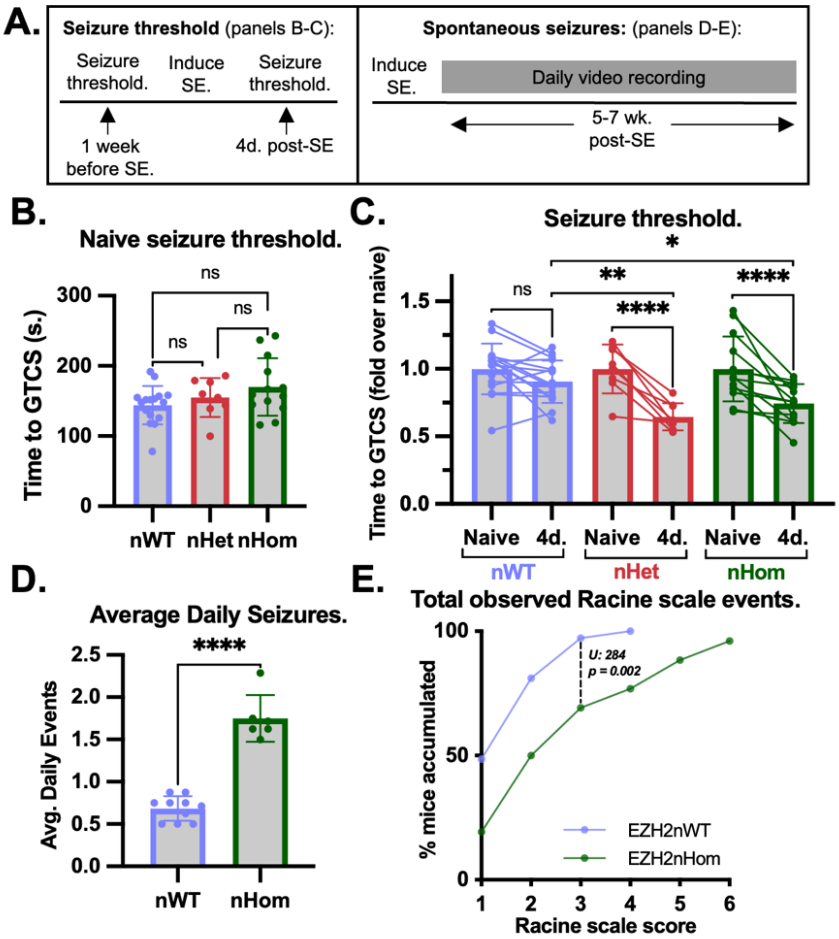

Fig. 1. EZH2 maintains seizure threshold after status epilepticus and mitigates spontaneous seizure frequency and severity. **(A)** Experimental paradigms for panels B-C and D-E. **(B)** Baseline fluorothyl seizure threshold data for C57BL6J EZH2nWT, nHet, and nHom mice. In naïve mice, deletion of EZH2 in neurons does not alter seizure threshold (one-way ANOVA; nWT:nHet p=0.471, nWT:nHom p=0.134, nHet:nHom p=0.471; n=8-16). **(C)** After induction of SE by KA injection, seizure threshold does not change robustly in EZH2nWT mice (p=0.061). EZH2nHet mice exhibit a 35% reduction in seizure threshold post-SE ($p<10^{-4}$), with thresholds 25% lower than kainate-injected EZH2nWT mice (p=0.003). EZH2nHom mice show a 25% reduction in seizure threshold post-SE ($p<10^{-4}$), with thresholds 17% lower than KA EZH2nWT mice (p=0.026) (2-way ANOVA; n=7-14). **(D)** FVB EZH2nWT and nHom mice were injected with KA to induce SE and video recorded from 5-7 weeks post-SE to count and score spontaneous seizure activity. Deletion of an EZH2 allele in neurons leads to a 2.5-fold increase in daily seizure events (unpaired t-test; $p<10^{-4}$; n=6-10). **(E)** Total observed Racine scale events for EZH2nHom and EZH2nWT mice were quantified as a frequency distribution. 50% of EZH2nWT mice had only Class I seizures, while 50% of EZH2nHom mice had Class I and II seizures (Mann-Whitney test; U:284, p=0.002; n=6-10).

RESULTS

Neuronal EZH2 maintains seizure threshold and protects against exacerbated epileptic phenotypes.

We previously identified the histone methyltransferase EZH2 as a potential driver of gene repression post-SE, and EZH2 protein was shown to be potently induced over a 10-day window post-SE in rats and mice across models of epilepsy. EZH2 induction was protective because pharmacological inhibition resulted in accelerated disease progression[23]. To determine the role of EZH2 in epilepsy, we crossed EZH2 floxed mice[36] with Syapsin1 Cre drivers[37] to delete EZH2 in mature neurons. Neuronal specificity of Cre expression was confirmed via crossing Syn1Cre with *flox*-STOP-*flox*-tdTomato mice and immunofluorescence (Fig. S1A).

Immunofluorescence and western blot analysis confirmed successful ablation of neuronal EZH2 post-SE. Fig. S1B-C show diminished induction of EZH2 on day 4 post-SE in mice lacking one EZH2 allele in neurons (EZH2nHet) or lacking both alleles (EZH2nHom). Staining for EZH2 confirmed reduced induction of neuronal EZH2 in EZH2nHet versus wildtype (EZH2nWT) mice (Fig. S1D, quantified in S1E).

We tested the impact of EZH2 deletion on fluorothyl seizure threshold acutely post-SE, as a correlation between fluorothyl seizure threshold[38] and the development of spontaneous seizures has been suggested[39-42]. We measured time to generalized tonic clonic seizure (GTCS) after exposure to the volatile chemoconvulsant fluorothyl in EZH2nWT, EZH2nHet, and EZH2nHom mice aged 4-6 weeks, before and after kainate-induced SE[43,44] (Fig. 1A). Loss of EZH2 alleles in neurons had no impact on seizure threshold in naïve mice (Fig. 1B), and induction of SE did not alter the seizure threshold of EZH2nWT mice on day 4 post-SE (Fig. 1C). In contrast, robust reductions in threshold were detected after SE in EZH2nHet mice (2-way ANOVA; Mean difference:55±8sec, $p<10^{-4}$) and EZH2nHom mice (Mean difference:46±8sec, $p<10^{-4}$). These were significant reductions compared to EZH2nWT mice (EZH2nWT:EZH2nHet: 28%, $p<0.01$; EZH2nWT:EZH2nHom: 20%, $p<0.05$). These data suggest that EZH2 is required to maintain fluorothyl seizure threshold post-SE.

We considered the possibility that EZH2 loss primed the mice to experience more severe responses to kainate injection, and it was this vulnerability to SE driving the observed reduction in mutant seizure threshold. However, we found no differences in time to first class V seizure and no correlation between time to first class V seizure and time to GTCS post-SE for either EZH2nWT (Pearson correlation; R^2:0.016, p=0.633), EZH2nHet (R^2:0.261, p=0.195), or EZH2nHom mice (R^2:0.152, p=0.209) (Fig. S2A-D).

To test the impact of neuronal EZH2 deletion on spontaneous seizures, we monitored behavioral spontaneous seizures in FVB EZH2nWT and EZH2nHom mice by video weeks five to seven post-SE (Fig. 1A). EZH2nHom mice exhibited a 2.5-fold increase in average daily seizure events compared to EZH2nWT mice (unpaired t-test; $p<10^{-4}$) (Fig. 1D). EZH2nHom mice also exhibited more severe Racine scale seizures than EZH2nWT mice (Mann Whitney test; U: 284, $p<0.01$) (Fig. 1E). These data support the hypothesis that neuronal EZH2 induction is a protective response post-SE.

EZH2 tempers induction of the JAK/STAT pathway post-SE in neurons.

To begin to understand the mechanism behind EZH2-mediated protection, we performed bulk RNAseq on whole hippocampal tissue from naïve and epileptic (4d. post-SE) EZH2nWT and EZH2nHom mice. Of the 10556 expressed genes, 6241 were found to be differentially expressed at an adjusted $p<10^{-2}$ (Likelihood Ratio Test) across the four conditions (saline, kainate, EZH2nWT, EZH2nHom). A community-based network approach was used to group genes into clusters. Leiden clustering generated 12 distinct groups (Fig. 2A). The grey, orange, gold, brown, skyblue, and purple clusters were generally repressed after SE, whereas the red, blue, indigo, yellow, and black clusters were generally increased. We focused on the Black cluster because these 439 genes manifested induction with SE in EZH2nWT mice but showed an exaggerated induction with SE in EZH2nHom mice. We reasoned that these would be genes whose expression is induced with SE but tempered in the presence of EZH2 post-SE, and undergo unfettered induction in the absence of EZH2.

To understand the nature of genes comprising the Black cluster, we performed an ontological analysis. The 439 Black cluster genes were compared to gene lists associated with terms in the KEGG, Reactome, Biocarta and Hallmark databases. (Fig. 2B). The ontology network (see Fig. S3A) highlights the innate immune response (NFkB, Interferon Gamma), microglial processes (Complement) and inflammation (IL6 Jak Stat3) amongst others. The term 'IL6 Jak Stat3' was of particular interest given that our previous work highlighted STAT3 as a driver of gene activation across models of epilepsy[23], and others have identified a role for the JAK/STAT pathway in epileptogenesis[27,32,45-48].

To determine which transcription factors and cofactors (hereafter together referred to as 'Factors') control expression of Black cluster genes, we used MAGIC[21]. STAT3 was the highest scoring Factor (Fig. 2D). When projected as a Gene Regulatory Network (GRN) (Fig. 2C) such that an arrow projects from Factor X to Factor Y if the gene encoding Factor Y is a transcriptional target of Factor X, STAT3 stood out as a central node. Thus, STAT3 had the highest in-degree, out-degree and total edge count (Fig. 2E) of any Factor in the

network. Finally, we assessed the Betweenness Centrality of the network[49] to determine which Factors might be critical for information flow in the GRN. STAT3 had by far the largest Betweenness Centrality of any Factor (Fig. 2F).

To ascertain whether the mouse Black cluster has a counterpart in human epilepsy, we used whole transcriptome data from 129 temporal lobectomy resections collected ante-mortem from human temporal lobe epilepsy (TLE) patients[23,50]. We used k-means clustering to generate 10 gene clusters from the 7658 genes co-expressed across all samples (brown, blue, purple, skyblue, grey, orange, indigo, green, yellow, red). To identify the human TLE cluster most similar to the mouse Black cluster, we performed Fisher exact tests to measure the degree of overlap between the 439 Black cluster genes, and the genes comprising each cluster of the human TLE dataset (Fig. 2G). The human Brown cluster showed the greatest overlap, sharing 65 genes in common with the mouse Black cluster (Fisher exact; Odds: 4.79, p=1.19E-20). We then performed ontological analysis on the genes in the human Brown cluster. The 850 genes were compared to gene lists associated with terms in the KEGG, Reactome, Biocarta and Hallmark databases. (Fig. 2H). The ontology network (see Fig. S3B) highlights inflammation (Cytokine Receptor Interaction/Complement/Innate Immune System) and interferon signaling (Interferon Gamma Response). Mirroring results of the black cluster, STAT3

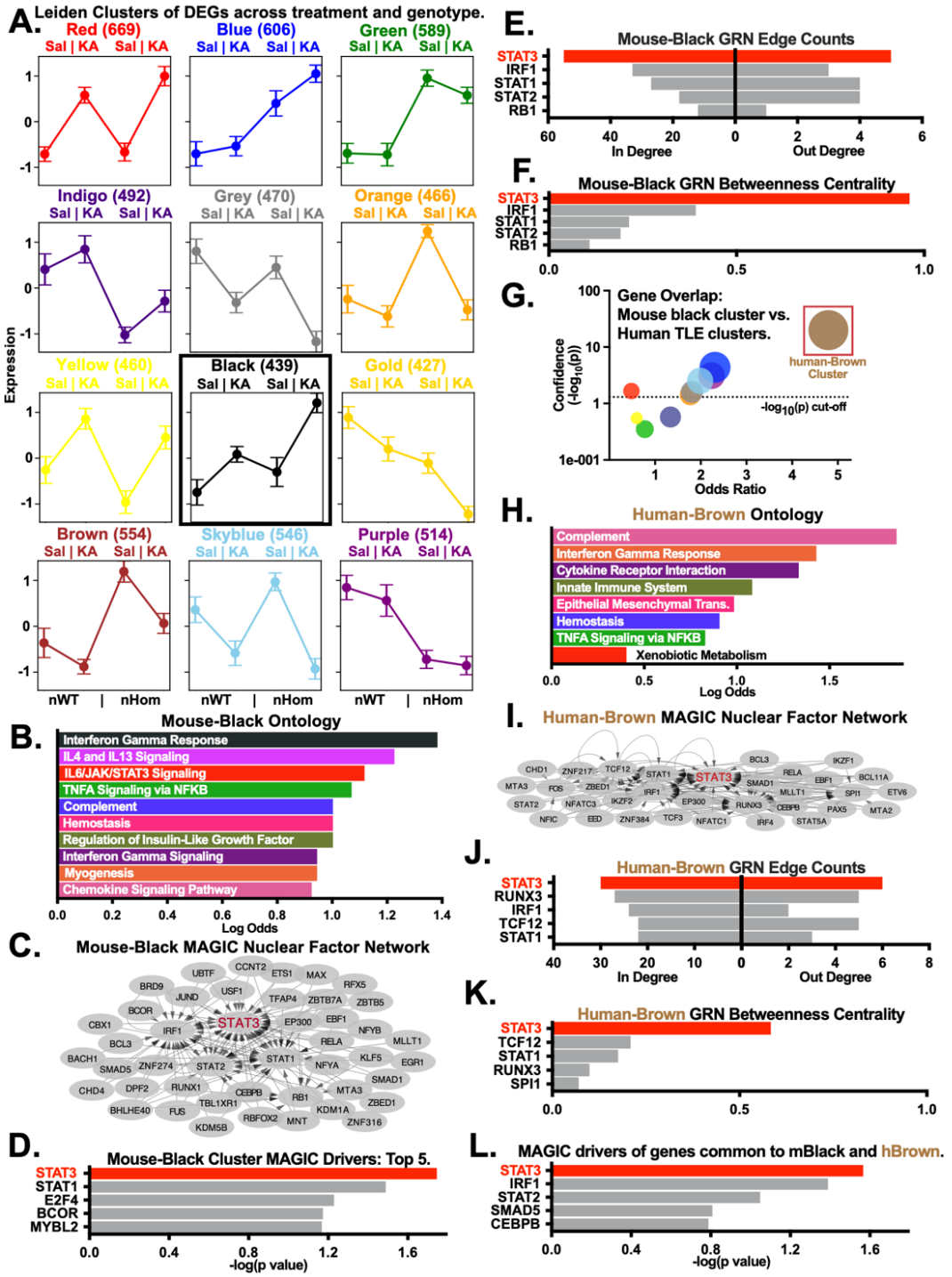

Fig. 2. STAT3 drives hyper-activation of pro-inflammatory gene networks post-SE in EZH2 knockout mice and human temporal lobe epilepsy. **(A)** Leiden clusters from 6241 differentially expressed genes (fold change >1.2x, adjusted p<0.01) across saline, kainate, EZH2nWT, and EZH2nHom conditions. **(B)** Ontological analysis of genes in the Black cluster highlights inflammatory processes. **(C)** MAGIC was used to determine which Factors control the expression of Black cluster genes, and positive hits were projected as a Gene Regulatory Network (GRN). **(D)** Top 5 Factors driving expression in the Black cluster sorted by –log(adjusted p value). **(E, F)** Factors were ranked by their in degree, out degree counts, and betweenness centrality. **(G)** Comparison of 10 human TLE k-means gene clusters to the mouse Black cluster by Fisher Exact test. Plotting -log(adjusted p) versus odds ratio of Fisher tests against the Black cluster shows that the Human Brown cluster is the most similar to the mouse Black cluster (Fisher exact; Odds:4.79, p(adj)=1.2×10^{-20}). Dotted line shows p=0.05. **(H)** Ontological analysis of genes in the human-Brown cluster. The 850 human-Brown cluster genes were compared to gene lists associated with terms in KEGG, Reactome, Biocarta, and Hallmark databases **(I)** MAGIC GRN for Factors driving the human-Brown cluster. **(J, K)** Factors were ranked by their in degree, out degree, and betweenness centrality. **(L)** STAT3 is the top driver predicted by MAGIC to drive expression of genes common to the mouse-Black and human-Brown clusters.

in the human Brown GRN had the highest in-degree, out-degree, and betweenness centrality of any Factor in the network (Fig. 2J-K).

MAGIC called STAT3 as the highest scoring Factor driving expression of the 65 genes co-expressed in early rodent epileptogenesis (mouse Black) and frankly epileptic human tissue (human Brown) (Fig. 2L). This data is consistent with the hypothesis that STAT3-mediated disease mechanisms that are activated acutely in a rodent model of epileptogenesis persist in chronic human epilepsy.

Transient activation of the JAK/STAT pathway after SE in WT mice has been reported by others[23,46] (and Fig. S4A-B, S5A-D). To test for a neuronal EZH2-dependent change in JAK/STAT signaling, we performed western blot analysis on hippocampal lysates from 4d. post-SE WT and EZH2 mutant mice (Fig. 3A-B). On day 4 post-SE, pY705-STAT3 was induced 2-fold in EZH2nWT mice ($p<0.01$) compared to naïve controls, 2.9-fold in EZH2nHet mice ($p<10^{-4}$), and 4.5-fold in EZH2nHom mice (2-way ANOVA; $p<10^{-4}$) (Fig. 3C-D). These results demonstrated an EZH2 gene dose-dependent hyperactivation of STAT3.

Given the involvement of STAT3 in regulating gene expression across acute rodent SE and chronic human epilepsy, we asked whether STAT3 reactivation occurred in chronic rodent epilepsy. We found that at 14 weeks post-SE, epileptic mice showed a 4.7-fold induction of pY705-STAT3 over naïve controls (unpaired t-test; $p<0.01$) (Fig. 3E-F).

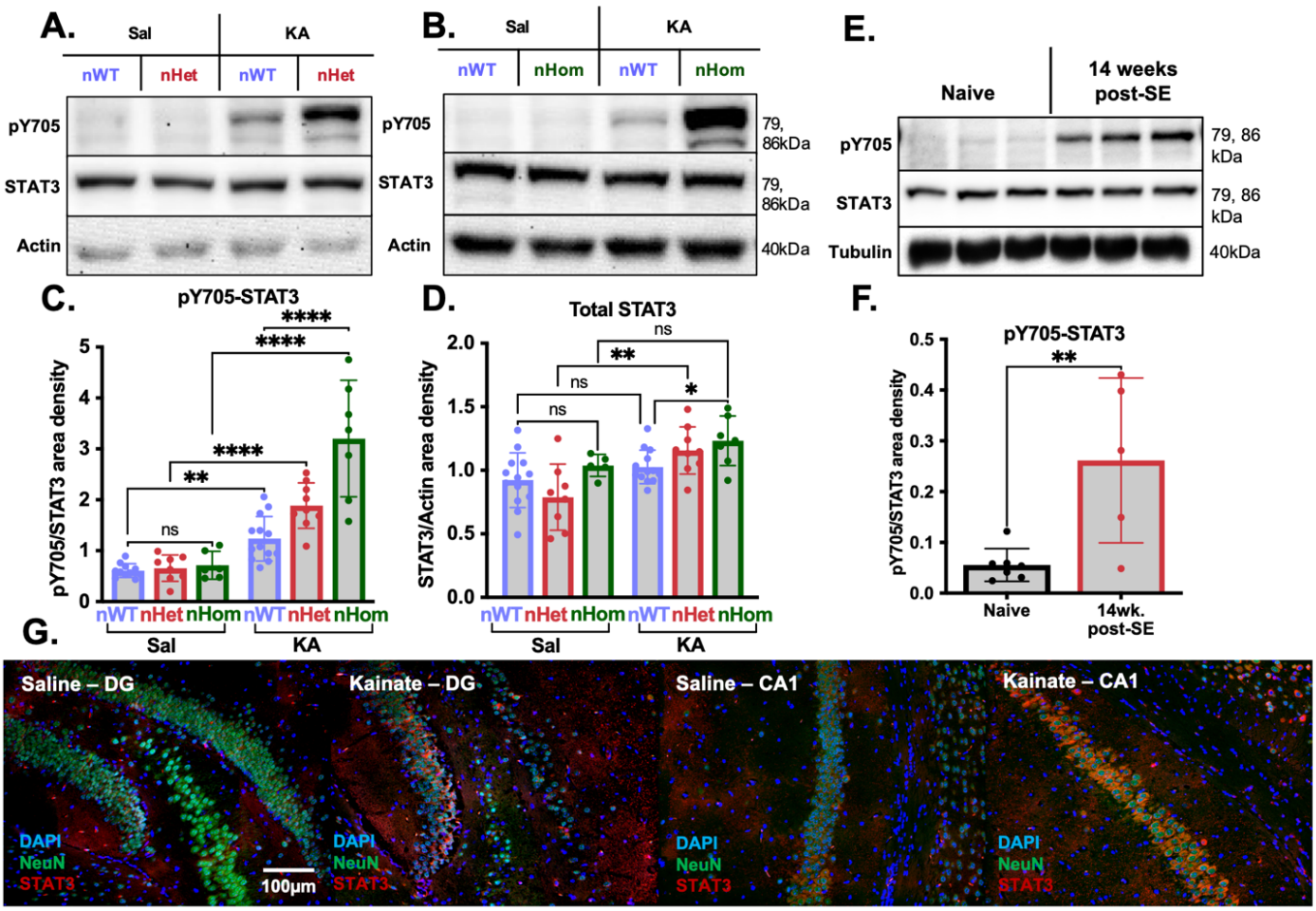

Fig. 3. JAK/STAT pathway components are hyper-activated in neurons of EZH2 knockout mice. EZH2nWT, nHet, and nHom mice were injected with saline or KA to induce SE; hippocampi were harvested on day 4 post-SE. **(A, B)** Representative western blots for pY705-STAT3, total STAT3, and beta-actin on day 4 post-SE. **(C)** pY705-STAT3 levels are unchanged across genotypes in naïve animals ($p=0.220$). pY705-STAT3 is induced by 2-fold in EZH2nWT mice ($p=0.022$), 2.9-fold in EZH2nHet mice ($p<10^{-4}$), and 4.5-fold in EZH2nHom mice post-SE ($p<10^{-4}$). pY705 levels in EZH2nHom mice post-SE are 2.6-fold greater than in EZH2nWT mice post-SE ($p<10^{-4}$) (2-way ANOVA; n=7-12). **(D)** Total STAT3 levels on day 4 post-SE. Total STAT3 is induced by 1.2-fold in nHom mice post-SE, compared to nWT mice post-SE ($p=0.041$). Total STAT3 is induced after seizures in nHet mice by 1.5-fold ($p=0.041$) (2-way ANOVA; n=7-12). **(E)** Representative western blots for pY705-STAT3, total STAT3, and beta actin in naïve and chronically epileptic mice at 14 weeks post-SE. **(F)** pY705-STAT3 is induced 4.7-fold in epileptic mice (unpaired t-test; $p=0.007$, n=5-7). **(G)** 20x images of the dentate gyrus (DG) and CA1 pyramidal cell layer (CA1). Hippocampal slices were collected on day 1 post-SE from saline- and KA-injected mice; immunofluorescence was performed to detect nuclear DNA, NeuN, and total STAT3.

To define the cell types in which STAT3 is expressed after seizures, we performed immunofluorescence with DAPI, NeuN, and total STAT3 antibodies on day 1 post-SE hippocampi taken from mice injected with saline or kainic acid (Fig 3G). We made use of the fact that the STAT3 gene is induced with STAT3 activation, and so elevated total STAT3 protein was a proxy for activated STAT3. In both the dentate granule and CA1 pyramidal cell layer, we observed a robust induction of total STAT3 in NeuN-positive cells.

EZH2 targets STAT3 via JAK1 to suppress JAK/STAT signaling.

STAT3 was a central factor in the Black cluster GRN whereas, surprisingly, EZH2 was not. In order to understand how STAT3 hyperactivation could have occurred in the absence of EZH2, shRNA was used to knock down EZH2 in the Neuro2A (N2A) neuronal cell line. We observed robust diminution of EZH2 in knockdown cells (shEZH2) (Fig. 4A, quantified by S6A) (unpaired t-test; 3.7-fold, $p<10^{-4}$). This was associated with a marked increase in pY705-STAT3 levels (unpaired t-test; 2.4-fold $p<10^{-4}$) (quantified by S6B). This result suggests that EZH2 suppresses STAT3 activation in a cell-autonomous manner without circuit level alterations.

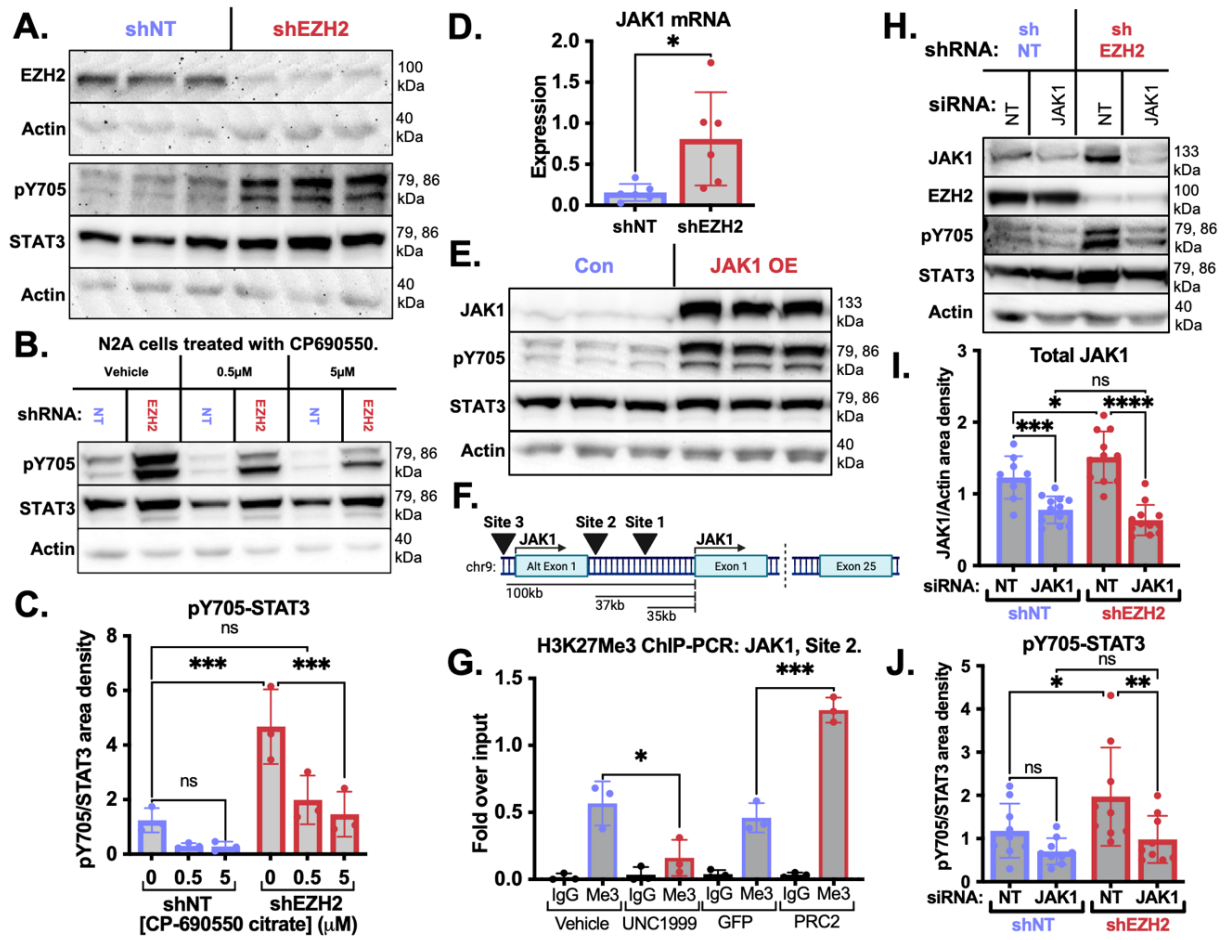

Fig. 4. EZH2 suppresses STAT3 activation via transcriptional repression of JAK1. N2A cells were stably transfected with EZH2 shRNA (shEZH2) or non-targeting shRNA (shNT). **(A)** Knockdown of EZH2 causes induction of pY705-STAT3 and total STAT3 protein (quantified in Fig. S6). **(B,C)** pY705-STAT3 activation in shEZH2 cells is inhibited with the JAK inhibitor CP690550 citrate. pY705-STAT3 is induced in vehicle-treated shEZH2 cells by 3.7-fold (p=0.0004). CP690550 treatment reduces pY705-STAT3 levels of KD cells by 2.3-fold (at 0.5μM) and 3.2-fold (p=0.0006) (at 5μM). At 0.5μM CP, pY705 levels in KD cells are reduced to that of untreated control cells (p=0.18) (2-way ANOVA; n=3). **(D)** JAK1 mRNA expression is induced by 5.1-fold in shEZH2 cells (unpaired t-test; p=0.019; n=6). (**E**) JAK1 protein is induced 5.5 fold (p=0.0008), and pY705-STAT3 by 6.7-fold (p=0.0004) in the absence of changes to total STAT3 upon transfection with FLAG-JAK1 compared to control transfection (unpaired t-tests; n=3). **(F)** Schematics depicting EZH2 binding sites on JAK1. **(G)** H3K27Me3 is enriched at Site 2 at the JAK1 locus. Chromatin IP (ChIP) on N2A cells treated with either vehicle or 10μM UNC1999 for 24 hours, or transfected with expression vectors GFP (control) of cotransfected with GFP-EZH2, SUZ12, and EED (PRC2). Results are graphed as fold H3K27Me3 over input. For JAK1 (Site 2), treatment with UNC1999 reduces H3K27Me3 enrichment by 3.5-fold (p=0.029), and PRC2 overexpression leads to a 2.7-fold increase in H3K27Me3 enrichment (p=0.0006) (unpaired t-tests; n=3). **(H)** Knockdown of JAK1 suppresses pY705-STAT3 activation in shEZH2 cells. shNT and shEZH2 N2A cells transfected with either non-targeting (NT) or JAK1 siRNA were subjected to western blotting to confirm JAK1 and EZH2 knockdown, and assess pY705-STAT3 levels. **(I)** Total JAK1 protein is induced in shEZH2 cells transfected with non-targeting siRNA by 1.2-fold (p=0.023), and reduced in both shNT (p=0.0005) and shEZH2 ($p<10^{-4}$) after JAK1 RNAi (2-way ANOVA; n=9-12). **(J)** pY705-STAT3 is induced in shEZH2:NTsiRNA cells by 1.7-fold (p=0.027) over shNT:NTsiRNA cells. JAK1 RNAi in shEZH2 cells reduces pY705-STAT3 by 2.5-fold (p=0.006), to the levels of shNT:NTsiRNA cells (2-way ANOVA; n=9-12).

To determine whether STAT3-upstream kinases are required for pY705-STAT3 induction in shEZH2 cell lines, we incubated cells with either WP1066 (an analogue of the JAK2 inhibitor AG490[51-53]) or CP690550 citrate (a small molecule inhibitor of JAK1/3 kinase activity[4,5,54]). WP1066 did not impact STAT3 phosphorylation in shEZH2 cells at any concentration tested (Fig. S7A-C). In contrast, 500nM CP690550 citrate resulted in a 2.3-fold (2-

way ANOVA; $p<0.01$) reduction of pY705-STAT3 in shEZH2 cells (Fig. 4B,C), rescuing pY705-STAT3 levels to that of vehicle-treated control cells. Even greater reduction occurred in the shEZH2 cells treated with 5μM CP690550 (3.2-fold, $p<10^{-3}$). CP690550 is a JAK inhibitor selective for JAK1 and JAK3, but JAK3 is not expressed in neurons or N2As (data not shown). We therefore tested whether JAK1 was elevated in the shEZH2 cells. Fig. 4D shows a 5.1-fold induction of JAK1 mRNA over control cells (unpaired t-test; $p<0.05$).

To determine whether induction of JAK1 is sufficient to induce STAT3 activation, we overexpressed JAK1 in N2A cells (Fig. 4E). JAK1 shows a 5.6-fold induction upon overexpression (unpaired t-test; $p<10^{-3}$), and pY705-STAT3 is induced by 6.7-fold (unpaired t-test; $p<10^{-3}$) in the absence of changes to total STAT3 (quantified in S8A-B). This suggests that CP690550 works to suppress STAT3 activation primarily through JAK1 downstream of EZH2.

To understand how EZH2 regulates JAK1 activity, we noted three putative EZH2 binding sites in the gene body and promoter region of JAK1 using ENCODE tracks in the UCSC Genome Browser[55] (Fig. 4F, Fig. S9A). We performed chromatin immunoprecipitation with anti-H3K27Me3 antibodies to determine whether EZH2 methylase activity was enriched at any of these sites. In Fig. 4G H3K27Me3 was enriched at site 2. Incubation of cells with UNC1999 (an EZH2 inhibitor[23,56]) for 24 hours resulted in a 3.5-fold loss of signal (unpaired t-test; $p<0.05$). Overexpression of EZH2, SUZ12, and EED (the core components of Polycomb) increased H3K27Me3 signal by 2.7-fold compared to overexpression of GFP as a control (unpaired t-test; $p<10^{-3}$). PAX2 and actin were immunoprecipitated as positive and negative controls for H3K27Me3 enrichment, respectively (Fig. S9B-C); ChIP-PCR results for JAK1 (Site 1), JAK1 (Site 3), JAK2, and STAT3 were also collected (Fig. S9D-G). None of these sites showed both a loss of H3K27Me3 enrichment after UNC1999 treatment and an increase in signal upon overexpression of Polycomb. These data are consistent with the hypothesis that EZH2 targets JAK1 transcription to temper activation of STAT3.

Finally, to corroborate our pharmacological findings, we transfected control and shEZH2 cells with siRNA against JAK1 or a non-targeting transcript, and validated knockdown of EZH2 and JAK1 by western blot (Fig. 4H). Total JAK1 protein is induced 1.2-fold upon EZH2 knockdown (2-way ANOVA; $p<0.05$). JAK1 RNA interference reduced JAK1 protein levels in both control (2-way ANOVA; 1.6-fold, $p<10^{-3}$) and shEZH2 cells (2.4-fold, $p<10^{-4}$) (Fig. 4I). Knockdown of JAK1 expression in shEZH2 cells was sufficient to rescue pY705-STAT3 levels to that of control cells transfected with non-targeting siRNA (2-way ANOVA; 2.0-fold, $p<0.01$) (Fig. 4J). These data support the hypothesis that CP690550 rescues STAT3 hyperactivation primarily through targeting JAK1.

Transient JAK inhibition acutely post-SE rescues epileptic phenotypes in EZH2 knockout mice.

To test whether loss of EZH2-mediated regulation of JAK1 contributed to the exacerbated disease progression observed in EZH2 mutant mice, we treated EZH2nWT and EZH2nHet mice with CP690550 after induction of SE. Because the hyper-induction of pY705-STAT3 in mutant mice occurred already at day 1 post SE (Fig. S10A-C), we injected mice with CP690550 or vehicle at 6, 12, and 24 hours post-SE. A cohort of mice was sacrificed three hours after final injection to assess hippocampal STAT3 activation by western blot to confirm target engagement (Fig. S10D-E). Consistent with the previous result (see Fig. 1B), neuronal deletion of EZH2 did not alter fluorothyl seizure threshold in naïve mice (Fig. 5B). CP690550 treatment raised the 4d. post-SE seizure threshold of EZH2nHet mice by 30 seconds (1-way ANOVA; $p<0.05$), rendering them indistinguishable from epileptic EZH2nWT mice (1-way ANOVA; $p>0.05$) (Fig. 5C). Thus, CP690550 rescued the increased seizure susceptibility phenotype associated with the loss of neuronal EZH2. These data support the hypothesis that EZH2 maintains seizure threshold post-SE by tempering activation of the JAK/STAT pathway.

To test whether transient CP690550 treatment immediately after SE mitigated long-term disease progression, mice were video recorded from weeks five to seven post-SE (Fig. 5A). CP690550 treatment immediately after SE reduced daily seizure frequency by 41% in EZH2nHom mice 5 weeks later (1-way ANOVA; $p<10^{-4}$). EZH2nHom seizure frequency was reduced from 2.6-fold above EZH2nWT to 1.5-fold (1-way ANOVA; $p<0.01$) (Fig. 5D). EZH2nHom mice treated acutely with CP690550 also exhibited a dramatic reduction in seizure

severity from untreated EZH2nHom mice (Mann-Whitney test; U:138.5, $p<0.01$), such that they were indistinguishable from WT mice (Fig. 5E).

To test whether CP690550 could rescue the increased seizure burden of EZH2nHom mice if administered during the chronic period, we recorded spontaneous seizures for two weeks post-SE in EZH2nWT and nHom mice starting 5 weeks post SE, followed by another 2-week recording period during which the EZH2nHom mice received daily injections of CP690550 (Fig. 5A). Daily CP690550 treatment in the chronic period reduced seizure severity and frequency by 80% in EZH2nHom mice (1-way ANOVA; $p<10^{-4}$) (Fig. 5F-G). Indeed, seizure frequency of EZH2nHom+CP mice was reduced to below EZH2nWT levels (1-way ANOVA; 1.9-fold, $p<10^{-3}$). Given the robust seizure suppression when administered during the chronic period, we considered the possibility that CP690550 may simply be an anticonvulsant. To test this, we measured seizure threshold using both flurothyl and PTZ (pentylenetetrazole)[57,58] in mice pre-treated with vehicle or CP690550 (15mg/kg, i.p.) thirty minutes prior to testing. This time was chosen because peak plasma levels are observed thirty minutes after oral administration[59] CP690550 pre-treatment had no effect on flurothyl or PTZ seizure threshold (Fig. S10F-G).

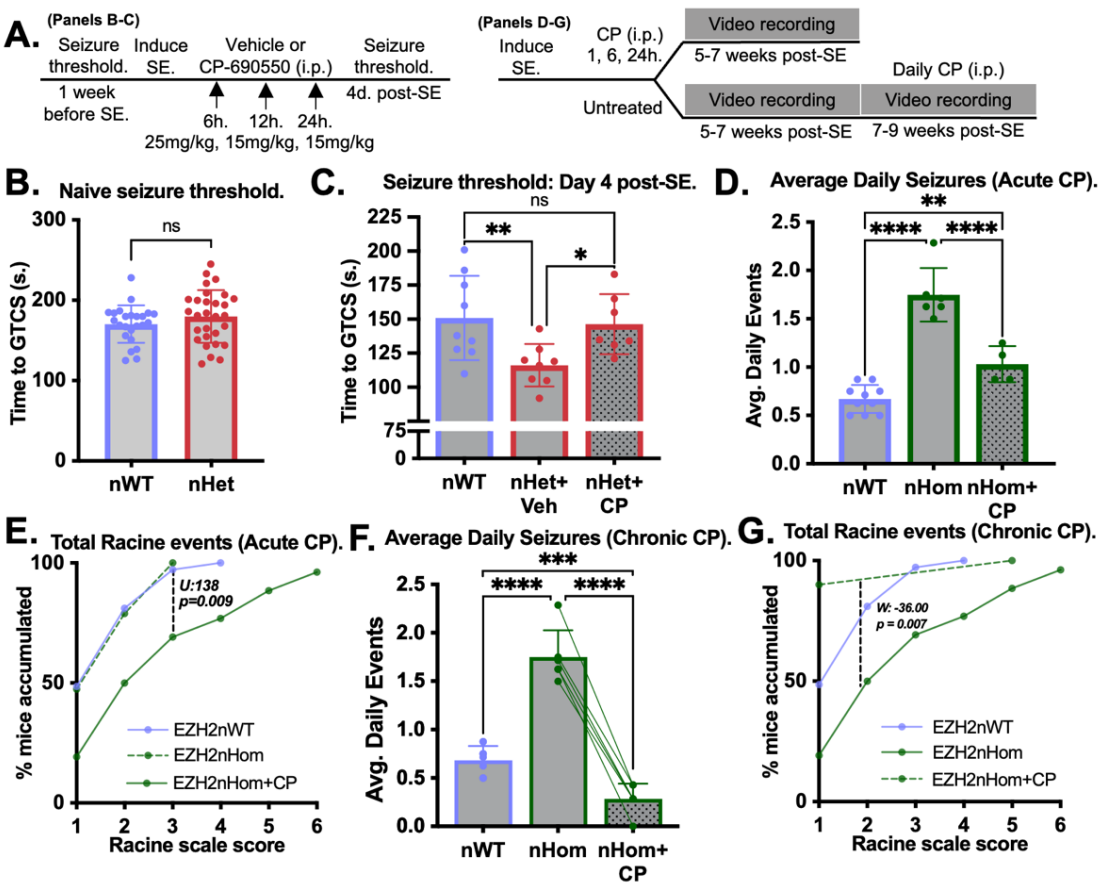

Fig. 5. JAK inhibition rescues seizure threshold reductions and spontaneous seizure burden in EZH2nKO mice. **(A)** (For panels B-C) Naïve seizure threshold was measured in C57 EZH2nWT and nHet mice one week prior to KA injections. **(B)** Deletion of an EZH2 allele does not alter seizure threshold in naïve mice (unpaired t-test; p=0.246; n=24-29). (**C**) nHet mice were injected with vehicle or CP690550 at 6, 12, and 24h. post-SE. Seizure threshold was measured 4 days post-SE. Untreated nHet mice show a 35 second reduction in seizure threshold (p=0.007) compared to nWT mice. CP690550 raises seizure thresholds of nHet mice by 30 seconds (p=0.025), extinguishing the difference between treated nHet and nWT mice (p=0.709) (1-way ANOVA; n=7-9). (**D**) FVB EZH2nWT and nHom mice received CP690550 or no treatment at 1, 6, and 24h. post-SE, and SRS activity was monitored by video from 5-7 weeks post-SE (see panel A). nHom mice treated acutely 6,12 and 24 hours post-SE with CP690550 exhibit a 41% reduction in daily seizures compared to untreated nHom mice ($p<10^{-4}$); a 34% difference remains between treated nHom mice and nWT mice (p=0.0073) (1-way ANOVA; n=4-10). **(E)** Racine scale events represented as a frequency distribution. Acute CP690550 treatment reduces seizure severity in nHom mice (Mann Whitney; U:138.5, p=0.009; n=4-10) to nWT levels (U:357, p=0.955). 50% of nWT and treated nHom mice had Class I seizures, while 50% of untreated nHom mice had Class I and II seizures. **(F)** SRS activity was monitored from 5-7 weeks post-SE, after which nHom mice received daily 10mg/kg CP690550 injections during monitoring from 7-9 weeks post-SE (see panel A). CP treatment reduced daily seizures by 80% in nHom mice ($p<10^{-4}$); treated nHom mice exhibit daily seizure frequencies 58% lower than nWT mice (p=0.0008) (1-way ANOVA; n=6-10). **(G)** Total observed Racine scale events represented as a frequency distribution. Daily CP690550 reduces seizure severity in nHom mice. 90th percentile seizure severities of nHom mice before and after treatment: 5.3 and 1, respectively (Wilcoxon matched pairs signed rank; W:-36.00, p=0.007, n=6). 90th percentile severity of WT mice: 2.6 (Mann Whitney test comparing nWT and treated nHom mice; U:119, p=0.042; n=6-10).

CP690550 profoundly suppresses electrographic and behavioral spontaneous seizures in epileptic WT mice.

CP690550 treatment during the chronic period reduced seizure frequency in EZH2nHom mice to below WT levels, so we tested its effect on WT epileptic mice. Chronic administration of CP690550 following intrahippocampal injection of kainate (IHKA) in WT epileptic mice significantly diminished spontaneous

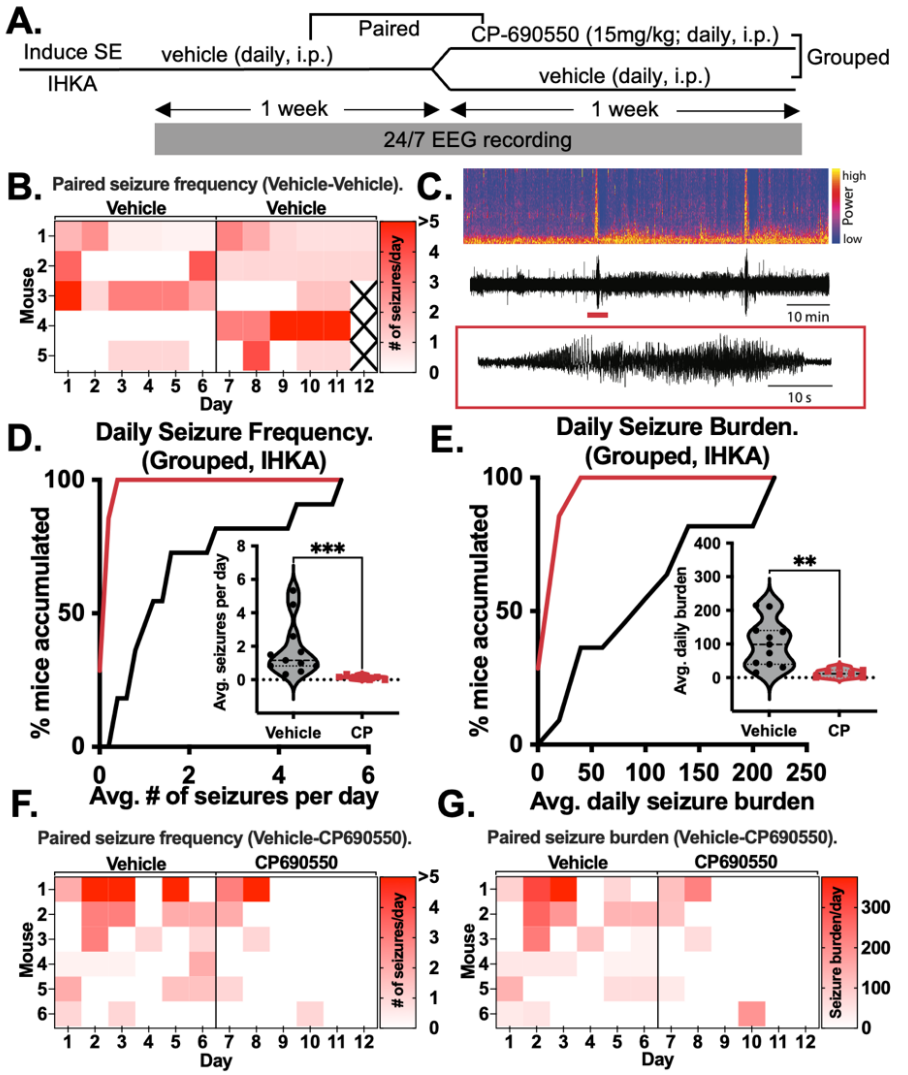

Fig 6. CP690550 profoundly suppresses spontaneous seizures in epileptic wildtype mice. **(A)** SE was induced via IHKA, and mice equipped with EEG headmounts. All under continuous EEG recording, vehicle (i.p.) was administered daily for one week followed by one week of daily vehicle or CP690550 treatment (i.p., 15mg/kg). **(B)** Vehicle-treated mice have spontaneous seizures across both weeks of the experiment. **(C)** Example power spectrum, trace, and seizure. **(D-E)** Grouped comparisons for seizure frequency and burden were displayed as a cumulative frequency distributions and violin plots. For cumulative graphs, bin centers are marked. 50% of vehicle-treated mice had up to 1.1 seizures per day on average, while 50% of CP-treated mice had up to 0.1 seizures per day. 50% of untreated mice showed seizure burdens of 99 per day, while 50% of treated mice showed burdens of up to 11 (Kolmogorov-Smirnov test; **Frequency:** D:0.9091, p=0.0003; **Burden:** D:0.7083, p=0.0162; n=5-12). **(F-G)** Heat maps display paired data for seizure frequency and burden. With the exception of one seizure observed on day 10, CP treatment eliminated seizures for the last four days of treatment.

recurrent seizures. In a paradigm involving one week of daily vehicle (i.p.) administration followed by an additional week of either vehicle or CP690550 injections (15mg/kg, i.p.) under continuous EEG recording (Fig. 6A), CP690550 treatment during the chronic period profoundly suppressed spontaneous seizures. Notably, 50% of vehicle-treated mice exhibited up to 1 seizure per day, with corresponding daily seizure burdens up to 99 (Fig. 6D-E). In contrast, 50% of CP690550-treated mice displayed up to 0.1 seizures per day, with daily seizure burdens up to 11. CP690550 treatment robustly reduced both spontaneous seizure frequency (Kolmogorov-Smirnov test; D:0.9091, $p<10^{-3}$) and burden (D:0.7083, $p<0.01$) in epileptic wildtype mice.

Additionally, while all animals experienced seizures during vehicle treatment, 17% of mice experienced no seizures at all during CP690550 treatment (Fig. 6F-G). Animals treated with vehicle throughout the experiment exhibited seizures consistently, contrasting with the profound reduction observed during CP690550 treatment (Fig. 6B, F-G).

Next, we continued exploration of CP690550's antiepileptogenic potential by inclusion of the systemic kainate model of epilepsy, as well as adopting video-based behavioral seizure monitoring. These experimental modifications aimed to generalize the efficacy of CP690550 across epilepsy models, minimize potential confounding effects introduced by headmount implantation, and prioritize clinically relevant seizure endpoints. Additionally, expansion of the observation period by two weeks after drug washout provided insights into any potential disease-modifying effects of CP690550 (Fig. 7A). Using a different model of epilepsy and method of seizure detection, we showed that CP690550 substantially curtailed seizures.

During weeks 11-12 post-SE, 75% of vehicle-treated mice exhibited up to 1.6 seizures per day and seizure burdens up to 10.7, while 75% of CP690550-treated animals had up to 0.05 seizures per day with seizure burdens up to 0.5 (Fig. 7B-C) (Kolmogorov-Smirnov test; **Frequency:** D:0.8333, $p<0.05$, **Burden:** D:0.8333, $p<0.05$). In paired analyses, vehicle-treated mice exhibited ongoing spontaneous seizure activity[60] (Fig. 7D,G), while CP690550 markedly suppressed seizures (Fig. 7E,H). CP690550 eliminated seizures in 60% of mice during treatment, and 40% of mice across both treatment and washout.

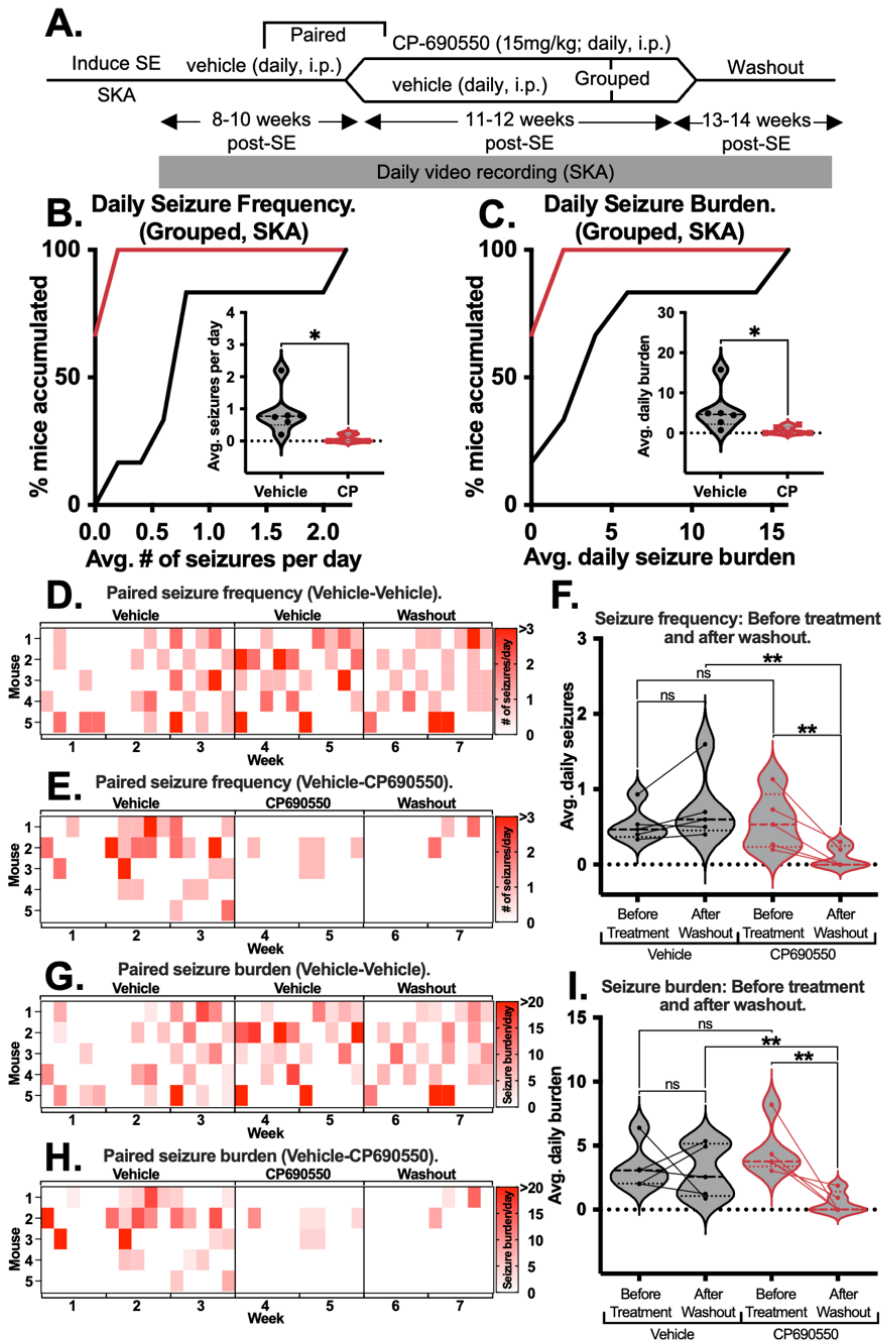

Fig 7. CP690550 profoundly suppresses spontaneous seizures in epileptic wildtype mice. **(A)** SE was induced via systemic kainate (SKA), and behavioral spontaneous seizure activity was monitored by video from weeks 8-14 post-SE. Vehicle (i.p.) was administered daily for three weeks followed by two weeks of daily vehicle or CP690550 treatment (i.p., 15mg/kg). Video recording continued for two weeks after drug washout. **(B-C)** Grouped comparisons for seizure frequency and burden were displayed as a cumulative frequency distributions and violin plots. For cumulative graphs, bin centers are marked. 75% of vehicle-treated mice had up to 1.6 seizures per day with daily burdens up to 10.7, while 75% of CP-treated mice had up to 0.05 seizures per day with daily burdens up to 0.5 (Kolmogorov-Smirnov test; **Frequency:** D:0.8333, p=0.015; **Burden:** D:0.8333, p=0.026; n=6-7). Heat maps display paired data for seizure frequency **(D-E)** and seizure burden **(G-H)**. CP690550 treatment eliminated seizures in 40% of mice during weeks 11-12 post-SE. Seizure frequency **(F)** and seizure burden **(I)** before treatment and after washout for vehicle- and CP690550-treated animals. Vehicle-treated mice show no robust change in seizure frequency (p=0.106) or burden (p=0.115) from before treatment to washout, while CP690550-treated mice exhibit an ongoing 83% reduction in frequency (p=0.005) and 88% reduction in burden (p=0.009) after drug is withdrawn. Compared to vehicle-treated mice during washout, this represents an 87% reduction in frequency (p=0.006) and 81% reduction in burden (p=0.002) (2-way ANOVA; n=5).

Drug washout occurred over the weekend following week 12 post-SE[59]. Mice treated with CP690550 continued to show profound seizure reduction for at least 2 weeks post-washout compared to vehicle-treated mice (2-way ANOVA; **Frequency:** 87% reduction, p<0.01, **Burden:** 81% reduction, p<0.01). This data supports the hypothesis that CP690550 exerts robust disease modification in a preclinical rodent model of epilepsy.

DISCUSSION

We show that CP690550 (Tofacitinib), an FDA approved, orally available drug with no known behavioral side effects, exerts a potent and enduring seizure-suppressive effect when administered transiently across rodent preclinical epilepsy models. We demonstrate that CP690550 shuts down a pro-epileptic gene network centered around STAT3 by inhibition of JAK1, an endogenous gene target of the protective chromatin modifier EZH2. We provide evidence that the STAT3 upstream kinase JAK1 is a novel therapeutic target for seizure suppression and disease modification across epilepsy models.

After status epilepticus, we find EZH2 protein is potently induced in hippocampal pyramidal and dentate granule neurons across models of epilepsy[23]. Previously, we reported that treatment of mice with the SAM-competitive EZH2 inhibitor UNC-1999 exacerbated spontaneous seizures, and here we find that deletion of EZH2 in mature neurons has the same effect. Induction of Polycomb group (PcG) proteins has been studied in association with other brain insults. For example, sublethal ischemic insults lead to induction of PcG proteins in mouse cortical neurons, and *in vitro* overexpression of PRC1 component BMI1 was sufficient to protect against oxygen-glucose deprivation-associated injury[61]. Further, sevoflurane (a volatile anesthetic that exerts positive allosteric modulation on $GABA_A$ receptors[62] and antagonizes NMDA receptors[63]) mediates the protective induction of EZH2 and H3K27Me3 to attenuate hypoxic-ischemic brain injury, reducing hippocampal autophagy and improving post-injury behavioral

assessments in rats. Intriguingly, these improvements are reversed when rats treated with sevoflurane also receive a dose of the EZH2 inhibitor GSK126[64]. These studies, along with our findings, point to a potentially general protective role for EZH2 in brain insults.

EZH2 deletion in neurons results in large transcriptomic changes that manifest after SE (Fig. 2). The mouse Black gene cluster houses genes whose expression are relatively unchanged in naïve EZH2nWT and EZH2nHom animals, induced after SE in EZH2nWT, and hyper-induced in EZH2nHom mice after SE. This pattern suggests that EZH2 might be responsible for tempering expression of genes in this cluster because its deletion results in their unfettered activation. The Black cluster ontological analysis produces terms associated with innate immunity, neuroinflammation, and the JAK/STAT pathway. Network analysis places STAT3 in the center of the Black GRN, and immunofluorescence confirms induction of STAT3 in neurons post SE. While activation of the JAK/STAT pathway in non-neuronal cells post-SE is well-characterized[26,47,65,66], the role of STAT3 in neurons, especially in epilepsy, has been less studied; thus the mechanisms of neurogenic inflammation post-SE are not clear[45]. Cytokines released from glial cells following seizures increase neuronal excitability[67], and type I IFNs increase excitability in neocortical pyramidal neurons via PKC[68]. Others report that seizure-induced activation of the JAK/STAT pathway reduces the number of gamma-aminobutyric acid (GABA) type A alpha1 receptors expressed in neurons following seizures, influencing GABA(A)R-dependent inhibition[27]; this group has also utilized pharmacological inhibition of STAT3[32] and genetic ablation of the STAT3 SH2 domain[45] to reduce spontaneous seizure frequency in rodent models of epilepsy. Thus, activation of neuroinflammatory pathways, including the JAK/STAT pathway, has been shown to modulate neuronal excitability. However, our work is the first to identify an endogenous protective mechanism induced by SE that works to temper JAK/STAT activation and associated neurogenic inflammation. Our's is also the first to demonstrate an enduring protective effect of targeting this pathway in chronic epilepsy after the onset of spontaneous seizures.

In order to understand the mechanism by which EZH2 suppresses STAT3 activation, and to rule out the possibility that STAT3 hyper-induction in EZH2 mutant mice might be a consequence of worsened disease progression more generally, rather than loss of EZH2 *per se*, we turned to an *in vitro* cell line model. Knocking down EZH2 in N2A cells results in induction of STAT3 Y705 phosphorylation. This activation is not via secretion of soluble factors as swapping media from control and knockdown cells fails to activate STAT3 (data not shown). WP1066, a JAK2 inhibitor[51-53] fails to suppress activated STAT3 in shEZH2 cells whereas CP690550 (a JAK1/3 inhibitor) (Fig. 4B-C) and direct knockdown of JAK1 (Fig. 4H-J) succeeds. Given that JAK3 is not expressed in these cells, we conclude that EZH2 tempers JAK1. Finally, we find that EZH2 directly interacts with the JAK1 locus (Fig. 4G). Increased activation of STAT3 at pY705-STAT3 as a result of EZH2 inactivation has also been observed in a transformed murine cell model of early T cell precursor acute lymphoblastic leukemia; EZH2 inactivation leads to enrichment of documented STAT3 target genes, increased expression of IL6RA, and an exaggerated pY705-STAT3 induction in response to IL6 stimulation[69]. STAT-upstream receptors and kinases are also regulated by EZH2. In prostate cancer EZH2 directly targets the interferon gamma receptor gene INFGR1 to dampen JAK2/STAT1 signaling, and EZH2 depletion restores expression of IFN target genes as well as STAT1 phosphorylation.[70]

Others have identified EZH2 as an activator of JAK/STAT signaling as well as a target of the pathway. When phosphorylated by AKT at serine 21, EZH2 disassociates from Polycomb to enhance STAT3 transcriptional activity through di-methylation of STAT3-K49 in glioblastoma cells[71-73]; we have performed western blotting to assess this posttranslational mark in mouse hippocampi post-SE and find no change in STAT3-K49Me2 after seizures or deletion of EZH2 (data not shown). Thus, this mechanism does not appear to play a role in N2As or the mouse brain. In NK/T-cell lymphoma, JAK3 phosphorylates EZH2 to mediate a switch in its function, promoting the transcriptional upregulation of oncogenes through the interaction of EZH2 and Pol-II[74]. To our knowledge, ours is the first report of EZH2 repressing JAK/STAT activation through JAK1.

Analysis of human TLE samples identifies a cluster of genes strikingly similar to the STAT3-driven mouse Black cluster; the human Brown cluster is a group of genes associated with innate immunity and neuroinflammation. Like the mouse Black cluster, the most influential driver of gene expression is STAT3. This is a possible explanation for why CP690550 suppresses disease whether it is administered shortly after SE (Fig. 5), or after the onset of spontaneous seizures (Fig. 6). The robust overlap between clusters of genes, one from frankly epileptic human samples and another from rodents, suggests a couple of points. Firstly, EZH2-

STAT3 mediated mechanisms identified in mice are clinically relevant. Secondly, the EZH2-STAT3 mechanism evoked acutely after insult plays a role later in chronic epilepsy; this is supported by the identification of STAT3 as a driver of gene expression, its transient activation acutely post-SE, and its reactivation in chronic rodent epilepsy (see Fig. 3).

EZH2nKO mice show both a decreased seizure threshold 4 days post SE as well as exaggerated seizure burden 5 weeks later compared to WT mice. CP690550 administration for 24 hours post-SE is sufficient to rescue both these phenotypes. This suggests that STAT3 hyper-induction drives seizure threshold reductions and spontaneous seizure increases in mutant mice. The observation that CP690550 profoundly suppresses spontaneous seizures when administered to EZH2nHom mice during the chronic period is consistent with reactivation of JAK/STAT signaling during the chronic period (Fig. 3E-G, 5F-G, 6C-K). This supports the possibility that mechanisms involved in disease initiation (e.g., activation of neuroinflammatory pathways) continue to perpetuate disease chronically. Leveraging the brain's own protective mechanism, we use CP690550 to buttress EZH2 suppression of JAK1. CP690550 profoundly suppresses seizures in WT epileptic mice across models of epilepsy. Following cessation of CP690550 treatment we observe robust disease modification for at least two weeks. Whether this disease-modifying effect is permanent will be the focus of future studies in the lab.

Anti-inflammatory drugs that have been used to suppress seizures in human patients[28-31] or have shown antiepileptogenic potential[32-35] in rodents pose several drawbacks: some or all are proposed only as supplemental therapies[28,29], risk worsened disease outcomes[29], show only transient effects[30], or are effective in only a subset of epilepsy patients[29,31]. We argue that an approach involving multiple animal models and multiple laboratories to identify drivers of disease increases the likelihood that druggable targets will be viable across human etiologies. With this approach we identify EZH2 as a protective negative regulator of the JAK/STAT pathway in epilepsy. Our current data is consistent with the hypothesis that CP690550 mitigates spontaneous seizures in chronic epilepsy and is disease-modifying. The cross-model approach by which we identified JAK1 and selected CP690550 suggests this drug may be useful across multiple epilepsies.

Recently, others find that neuron-specific deletion of the STAT3 SH2 domain plateaus, but does not reduce, seizure frequency in chronic epilepsy[45], whereas CP690550 treatment greatly reduces seizures. The explanation for this difference may be that there is incomplete ablation of STAT3 in their model, or it may suggest that the more robust therapeutic effect of CP690550 is attributable to JAK/STAT pathway suppression in non-neuronal cells (e.g., peripheral immune cells, microglia, etc.) as well as neurons.

The JAK/STAT pathway is likely one of many processes orchestrating disease progression. The data presented here represents the first evidence that EZH2 regulates JAK/STAT function through JAK1/STAT3 in epileptogenesis to suppress disease progression. Transient treatment with CP690550 not only mitigates exaggerated disease in EZH2 mutant mice, but is seizure suppressing and chronically disease modifying in WT mice in two different epilepsy models. Together, these data suggest an ongoing interplay between EZH2 and the JAK/STAT pathway, starting in early epileptogenesis and persisting in chronic epilepsy.

We conclude that EZH2 tempers the JAK/STAT pathway in epilepsy as a protective response but is ultimately overwhelmed. Buttressing this protective program with the FDA approved, orally available drug CP690550 thwarts disease progression and offers a novel therapeutic approach to treating epilepsy.

METHODS

Bioinformatics

Reads were mapped to the mm39 build mouse genome and subjected to Likelihood Ratio Tests using Deseq2[75]. Transcripts per million were calculated and genes were classified as expressed if they had at least 3 TPM in all samples of any one of the 4 conditions (saline:WT, kainate:WT, saline:EZH2nHom, kainate:EZH2nHom). Deseq2 output was then filtered for only expressed genes and adjusted p-values were recalculated for the reduced number of genes. Genes with an adjusted $p<.01$ and 1.2-fold change were subjected to Leiden clustering with resolution=0.5 using the scanpy Leiden tool[76]. Ontology was performed on all clusters using Ontomancer (manuscript in preparation). Briefly, Biocarta, Hallmark, KEGG, and Reactome

.gmt files were downloaded from https://www.gsea-msigdb.org/gsea/downloads.jsp. Gene sets associated with every term in the databases were collected. For each Leiden cluster, Scores (S_t) for each term, t, were calculated as:

$$S_t = \sqrt{(\log\ O_t)^2 + (-\log P_t)^2}$$

Where O_t and P_t, are the odds ratio and p values from Fisher exact tests for the overlap of Leiden cluster genes and genes for each term t. Only terms with odds ratios>1 and p values<0.05 were kept for further analysis. For each term, a gene list is generated containing the overlap of genes in the cluster and term, G_t. A term x term similarity matrix was generated where similarity between term i and j is the Fisher exact test log odds ratio $O_{i,j}$ for the intersection of genes in the terms G_i and G_j. This was converted to a network where nodes are terms. Edge weights were calculated as:

$$weight = (\log(O_{i.j}) / \max \log O)^6$$

Where max log odds is the maximum log odds value across all comparisons. The 6 power was used to separate nodes for visualization. Networks were generated using the scanpy Leiden tool with resolution=2. Each community was named after the highest scoring term in that community. Networks were visualized via Python's networkx and Plotly tools.

MAGIC was performed on all clusters essentially as described[21] but with r=1, and GTFs were ignored. GTFs were defined as any ENCODE Factors containing the strings "TBP", "POL", "GTF", or "TAF".

Gene Regulatory Network was projected using Cytoscape[77] using MAGIC outputs. Factors were connected to their targets with edges defined as ChIP signal extracted from the Target Folder generated by MAGIC. Target genes of Factors that were not themselves Factors were removed to generate the GRN. Network statistics were calculated in Cytoscape[77].

Analysis of human TLE expression data.

GSE63808[50] from GEO contained 129 transcriptomes from resected hippocampal TLE tissue. Probes with an Illumina p-value<0.05 in at least 20% of samples were retained in the analysis; the probes were consolidated to gene symbols by taking the median probe expression value per symbol. These 9076 genes formed the background list for ontological and MAGIC analyses. Expression values were normalized by the median expression value in that sample. Genes kept for further analysis exhibited variance greater that the median coefficient of variance across all samples. The resulting 7658 unique genes were subjected to k-means clustering using the k-means tools from Sci-kit learn[78] to divide genes into 10 clusters (brown, blue, purple, skyblue, grey, orange, indigo, green, yellow, red).

Overlap between each of the 10 human TLE clusters with mouse Black cluster genes was measured by Fisher exact test with the Benjamini-Hochberg correction for multiple comparisons. Ontological and MAGIC analyses were performed on the highest-scoring human Brown cluster as described in the previous section.

Cell culture.

Growth conditions. Cells were grown in 5% CO_2 at 37°C. Neuro2a cells were grown in MEM (#10-009-CV Corning, Manassas, VA) with 1.0g/L glucose, 1.5g/L L-Glutamine, and 10% fetal bovine serum (#26140-079 Gibco, Grand Island, NY).

Lentiviral and siRNA knockdown. Stable EZH2 knockdown in Neuro2a cells for western blot and RNA analysis was achieved using SMARTvector lentiviral delivery of shRNA per the manufacturer instructions. Puromycin selection began 48 hours after infection and maintained during cell expansion and experimentation. SMARTvector lentiviral mouse EZH2 mEF1a-TurboRFP shRNA (#V3SM7592-232015353, Dharmacon, Lafayette, CO) targeted the sequence *ATCGTAGTAAGTACCAATG*, and non-targeting mEF1a-TurboRFP control particles (#S10-005000-01) were used as an infection control. Transient JAK1 knockdown in Neuro2a

cells was accomplished using ON-TARGETplus Human JAK1 siRNA (#L-003145-00-0005, Dharmacon). Control cells were transfected with the ON-TARGETplus Non-targeting control pool (#D-001810-10-05, Dharmacon). Transfections were performed with RNAiMAX lipofectamine transfection reagent (#13778030, Invitrogen).

PRC2 and JAK1 overexpression. For overexpression of Polycomb, all plasmids were ordered and modified (if necessary) from Addgene (Watertown, MA). Control cells were transfected with pAdtrack-CMV (#16405). To overexpress PRC2, cells were transfected with pCMVHA-hEZH2 (#24230), pCMVHA-EED (#24231), and pCMVHA-SUZ12 (#24232). The EZH2 plasmid was modified in-house to produce an HA-EZH2-GFP fusion protein. To overexpress JAK1, cells were transfected with FLAG-JAK1 (#174572), and controls were transfected with pAdtrack-CMV. All transfections were carried out with Lipofectamine LTX reagent with PLUS reagent (#15338100, Invitrogen).

Animal care

All animal procedures and experiments were performed with approval from the University of Wisconsin-Madison School of Medicine and Public Health Instructional Animal Care and Use Committee, or the Institutional Animal Care and Use Committee of Emory University, as appropriate, and according to NIH national guidelines and policies.

Transgenic mice. Cre-driver and EZH2 floxed mice were ordered from Jackson Laboratories (#003966, #022616, Bar Harbor, ME). Mice were bred on a C57BL6 background. Using the previously described Synapsin1-Cre system[37] *EZH2*$^{-/-}$; *Syn1Cre*$^{+/-}$ (EZH2nHom) mice were generated by mating *EZH2*$^{flox/flox}$*; Syn1Cre*$^{+/-}$ females with *EZH2*$^{flox/flox}$ males. *EZH2*$^{+/-}$*; Syn1Cre*$^{+/-}$ (EZH2nHet) mice were generated by mating *EZH2*$^{flox/+}$*; Syn1Cre*$^{+/-}$ females with *EZH2*$^{flox/flox}$ and *EZH2*$^{flox/+}$ males [36]. *EZH2*$^{+/+}$*; Syn1Cre*$^{+/-}$ (EZH2nWT) mice were generated from mating pairs containing an *EZH2*$^{flox/+}$ male. To assess Cre expression, we used a reporter mouse with a lox-P flanked STOP cassette preventing transcription of tdTomato (#007909 Jackson Laboratories) [79]. Reporter males were bred with *Syn1Cre*$^{+/-}$ females to generate Cre-positive animals and Cre-negative controls.

Repeated low-dose KA model. Male and female C57BL6 and FVB mice were bred and housed under a 12-hour light/dark cycle with access to food and water *ad libitum*. Mice were allowed to reach 4-6 weeks of age (C57BL6) 5-7 weeks of age (FVB) before undergoing experimentation. Kainate injections were performed at the same time of day (~10 A.M.), and mice were returned to home cages before the start of the dark cycle (~5 P.M.). Mice were housed with littermates for the duration of the experiment, with males and females separated at weaning.

We used a repeated low-dose kainate mouse model to induce SE. To begin, mice were weighed and singly housed in observation chambers for the duration of the injections. Mice were injected intraperitoneally (i.p.) with 5.0mg/kg synthetic kainic acid (KA) dissolved in 0.9% saline (#7065, Tocris Bioscience, Bristol, United Kingdom). At twenty-minute intervals, mice were given 5.0mg/kg injections of KA up to the third injection. The dosage was then reduced to 3.75mg/kg. Animals continued to receive 3.75mg/kg injections of KA every twenty minutes until each reached SE. The subsequent KA injection was skipped if an animal experienced two or more Class V seizures within a single twenty-minute interval. Injections resumed for the next round, unless the animal reached SE. During induction of SE, seizures were scored using a modified Racine Scale[80] where I = freezing, behavioral arrest, staring spells; II = head nodding and facial twitches; III = forelimb clonus, whole-body jerks or twitches; IV = rearing; V = rearing and falling; VI = violent running or jumping behavior. Animals were considered to have reached SE after experiencing at least five Class V or VI seizures within a 90-minute window. KA mice were observed for 1-2 hours after SE. Animals were injected with 0.9% saline (s.c.), and soft gel food was provided in home cages. In the days following injection, animals were weighed and injected with 0.9% saline (s.c.) if body weight decreased by more than 0.5g.

Pilocarpine model of status epilepticus. Adult C57BL6 mice (8-12 weeks old, Charles River) were injected with terbutaline (4 mg/kg ip, Sigma T2528) and methylscopolamine (4 mg/kg ip, Sigma S8502) to alleviate respiratory and cardiovascular effects of pilocarpine, then 30 min later received saline or pilocarpine (280 mg/kg i.p. as free base, Sigma P6503) as described[34]. After 1 hour of SE, seizures were interrupted by diazepam (10 mg/kg ip).

742
743 **IHKA model of status epilepticus.** The intrahippocampal kainic acid (IHKA) model was employed to
744 generate chronically epileptic mice as previously described[81]. Kainic acid (100 nL of 20 mM; vIHKA) or vehicle
745 (100 nL of sterile saline; vIHSA) was stereotaxically injected into the hippocampus using the following
746 coordinate (from Bregma): 3.6 mm posterior, -2.8 mm lateral, and 2.8 mm depth. Only mice which experienced
747 status epilepticus and went on to develop spontaneous recurrent seizures were used in the current study.
748
749 **Fluorothyl and PTZ seizure threshold testing.** Male and female C57BL6 mice were bred and housed
750 under a 12-hour light/dark cycle with access to food and water *ad libitum*. Animals were allowed to reach 4-6
751 weeks of age before undergoing experimentation. Fluorothyl seizure threshold tests were performed at the
752 same time of day (~10 A.M.), and mice were returned to home cages before 5 P.M. Mice were housed with
753 littermates for the duration of the experiment, with males and females separated at weaning. All seizure
754 threshold tests were video recorded, and seizure behavior was scored by a blinded observer. Two tests per
755 mouse were performed: the first at one week prior to kainate injections and the second at four days post-SE.
756 Seizure threshold tests were performed on male and female EZH2nWT, EZH2nHet, and EZH2nHom
757 mice using 100% bis(2,2,2-trifluoroethyl) ether (#287571, Sigma-Aldrich, St. Louis, MO). All tests were
758 performed in a fume hood. Mice were placed in an airtight 10L. Plexiglas chamber (8.5"X10.75"X6.75").
759 Fluorothyl was infused into the chamber via a peristaltic pump at a rate of 40μL/minute onto a piece of
760 Whatman filter paper placed at the top of the chamber. The time to generalized tonic clonic seizure (GTCS)
761 was recorded from the start of fluorothyl infusion. Mice reached GTCS when they exhibited a complete loss of
762 postural and motor control. After experiencing a generalized tonic clonic seizure, mice were rapidly removed
763 from the chamber, and fluorothyl infusion was terminated. Mice were transferred to a recovery cage and kept
764 isolated until motor control and normal behavior returned (~10 minutes). Mice were returned to home cages
765 after recovery. PTZ was dissolved at 5mg/mL in 0.9% normal saline, and a single 45mg/kg dose was
766 administered (i.p.). Time to generalized tonic clonic seizure was recorded.
767
768 **Long-term video monitoring for spontaneous seizures.** Male and female FVB mice were bred and
769 housed under a 12-hour light/dark cycle with access to food and water *ad libitum*. Animals were allowed to
770 reach 5-7 weeks of age before undergoing kainate injections. Starting at either week 5 or week 7 post-SE,
771 video recording for spontaneous seizures was performed at the same time of day (~10 A.M.), and mice were
772 returned to home cages before 5 P.M. Mice were singly housed in observation chambers for the duration of
773 recording with access to food and water. During daily CP690550 treatment, mice were weighed and injected
774 daily before recording began. Videos were reviewed and scored by an experimenter blinded to treatment and
775 genotype using the aforementioned modified Racine scale. In the final experiment described by Figure 7, only
776 Racine class III-VI seizures were recorded. For each mouse, daily seizure burden was calculated as: (Total #
777 of seizures * Average seizure duration (s))/(Total recording hours).
778
779 **CP690550 citrate treatment of KA mice.** Following kainate injections, an independent researcher (not
780 the experimenter) randomly assigned mice to drug and vehicle conditions, and prepared both solutions. Drug
781 and vehicle solutions were coded as "A" or "B." CP690550 citrate (tofacitinib citrate) (#4556, Tocris Bioscience,
782 Bristol, United Kingdom) was dissolved in a solution of 70% saline (0.9%)/15% ethanol/15% DMSO. The 70%
783 saline/15% ethanol/15% DMSO solution was administered as vehicle. The independent researcher provided
784 the blinded experimenter with the drug solutions and a list of all mice assigned to group A or B; this researcher
785 did not participate in any seizure threshold testing or spontaneous seizure video scoring. CP690550 or vehicle
786 was delivered to mice intraperitoneally at 6, 12, and 24 hours or 1, 6, and 24 hours post-SE. The drug doses
787 for each of these time points, respectively, were 25mg/kg, 15mg/kg, and 15mg/kg.
788
789 **Continuous EEG recording and seizure detection.**
790 At the time of stereotaxic IHKA or IHSA injections, mice were implanted with chronic EEG recording
791 headmounts (Pinnacle Technology, cat. #8201) which were affixed to the skull with 4 screws: 2 screws serving
792 as EEG leads placed in the anterior and posterior cortex, 1 as a reference ground, and 1 as the animal ground.
793 The headmounts were secured with dental cement. 24/7 EEG recordings were collected at 4 KHz using a
794 100X gain preamplifier high pass filtered at 1KHz (Pinnacle Technology, cat. #8292-SE) and tethered turnkey
795 system (Pinnacle Technology, cat. #8200).
796 Seizures were detected using a custom analysis pipeline developed in-house in python (seizy;
797 https://github.com/neurosimata/seizy) as previously described[81]. Briefly, EEG traces were automatically

detected using a thresholding method from traces that were downsampled (decimated) to 100 Hz and divided into 5 second segments. Power (2-40 Hz) and line length were used to identify seizures. Seizures were only included if two consecutive 5 second segments were classified as seizures (minimum 10 seconds length) and were manually verified by an experienced investigator with expertise in electrographic seizure detection. Seizure frequency was calculated as the # of seizures per day by measuring total number of seizures a mouse had over a 24-hour period. The average seizure duration was calculated by taking the mean seizure duration for each mouse in each recording period. For each mouse, seizure burden was calculated as: (Total # of seizures * Average seizure duration)/(Total EEG recording hours).

Tissue isolation and homogenization

After KA seizure induction and/or treatment with CP690550 citrate, animals were sacrificed by rapid decapitation. Whole hippocampal hemispheres were harvested and flash-frozen in liquid nitrogen or on dry ice. Hippocampal tissue was lysed in Radioimmunoprecipitation Assay Buffer (RIPA: 50mM Tris, 150mM NaCl, 1% nonidet P-40, 0.5% sodium deoxycholate, 0.1% SDS) with mammalian protease inhibitor (1:1000, Sigma or 1860932 ThermoScientific) and phosphatase inhibitor (1:1000, Sigma or 78428 ThermoScientific). Protein from cell lines was harvested in Triton lysis buffer (3% 5M NaCl, 10% glycerol, 0.3% Triton X-100, 5% 1M Tris pH8.0) after PBS washes. Tissue was homogenized in lysis buffer by probe sonication (Fisher Scientific, Sonic Dismembrator, Model 100, Hampton, NH) on power 3 for two rounds, with 10 pulses per round. Supernatants were isolated by centrifugation and quantified using the DC Protein Assay (Bio-Rad, Hercules, CA) or BCA assay (ThermoScientific 23227). Protein extracts were stored at -80˚C. 5x loading buffer (0.5mM Tris, 10% SDS, 50% glycerol, 10mM EDTA, and 1% beta-mercaptoethanol) was added to each sample to reach a 1x final concentration. Extracts in loading buffer were boiled at 95˚C for 5 minutes and stored for up to one month at -20˚C until run on an acrylamide gel.

Western blotting

Protein extracts in loading buffer were loaded at 20µg per lane and resolved by electrophoresis in hand-poured acrylamide gels with a 5% acrylamide stacking layer (125mM Tris pH6.8, 5% acrylamide, 0.01% ammonium persulfate, 0.01% SDS, 0.01% TEMED) and an 8% acrylamide separating layer (375mM Tris pH8.8, 8% acrylamide, 0.015% ammonium persulfate, 0.015% SDS, 0.08% TEMED). Gels were transferred to polyvinyl difluoride membranes (PVDF; Millipore, Bedford, MA) using Tris-glycine transfer buffer (20mM Tris, 1.5M glycine, 20% methanol). Membranes were blocked with 5% bovine serum albumin (Fisher Scientific, Fair Lawn, NJ) diluted in low-salt Tris-buffered saline (w/w TBST; 20mM Tris pH7.5, 150mM NaCl, 0.1% Tween 20) with mammalian protease inhibitor (1:2000) and phosphatase inhibitor (1:2000), or Odyssey blocking solution (LI-COR, 927-60001) for 1 hour at room temperature. Primary antibodies were diluted in the same blocking buffer and incubated with membranes overnight at 4˚C. Antibodies include: EZH2 (1:1000, #5426 Cell Signaling, Danvers, MA), pY705-STAT3 (1:2000, #9145 Cell Signaling), STAT3 (1:1000, #12640 Cell Signaling), JAK2 (1:1000, #3230 Cell Signaling), JAK1 (1:1000, #3344S Cell Signaling), STAT1 (1:1000, #14994 Cell Signaling), pS727-STAT1 (1:1000, #8826 Cell Signaling), STAT2 (1:1000, #72604 Cell Signaling), pY1007/08-JAK2 (1:500, ab32101, Abcam, Cambridge, UK), Tubulin (1:1000, #T9026 Sigma-Aldrich), and Actin (1:10,000, #691001 MP Biomedicals). The next day, the membranes were washed three times in 1X TBST and incubated with horseradish peroxidase-conjugated goat-anti-mouse or -rabbit secondary antibodies for one hour at room temperature (1:10,000, Invitrogen #31430, #31460, Rockford, IL). Membranes were subsequently washed three times in TBST, and membranes were developed in SuperSignal West Femto ECL reagent (ThermoFisher, Waltham, MA). Bands were imaged using a ChemiDoc-It Imaging System (UVP Vision-Works, Upland, CA) and quantified using UVP Vision Works software or ImageJ. Band intensities were graphed and analyzed using Prism 9 software (GraphPad Software, La Jolla, CA).

RNA extraction and clean-up for whole hippocampal RNAseq

Hippocampi were harvested from saline- and kainate-treated EZH2nWT and EZH2nHom mice on day 4 post-SE (n=4-5 per treatment/genotype). RNA was extracted from hippocampal tissue with Trizol (#1559602, Life Technologies, Carlsbad, CA), and concentration was determined by spectrometry. This was followed by a treatment with DNase (#AM2238, Invitrogen). RNA clean-up was carried with the RNeasy Mini Kit (#74104,

853 Qiagen, Hilden, Germany). Purified samples were submitted to the Gene Expression core at the University of
854 Wisconsin-Madison Biotechnology Center for library preparation and sequencing (https://biotech.wisc.edu).
855
856 **Chromatin immunoprecipitation and qPCR**
857
858 4% formaldehyde was used to crosslink proteins to chromatin before neutralization of the reaction in 125mM
859 glycine, and washes in 1X PBS (pH 7.4). Chromatin was fragmented in Triton-X lysis buffer and 1:100
860 protease inhibitors; lysates were sonicated and centrifuged to remove cell debris. Protein concentration of the
861 supernatant was quantified with BioRad Bradford assay reagent (#5000006). Chromatin was incubated
862 overnight at 4 degrees Celsius with antibodies against H3K27Me3 (#9733 Cell Signaling) or rabbit IgG. The
863 next day, protein A/G magnetic beads (#88803, ThermoScientific) were blocked in BSA and salmon sperm
864 DNA while chromatin samples were centrifuged, after which chromatin-antibody complexes were added to the
865 beads to incubate. Washes were performed in a low-salt ChIP buffer (1% SDS, 1% Triton X-100, 0.4% 500mM
866 EDTA, 2% 1M Tris pH8.1, 3% 5M NaCl). Decrosslinking buffer (1% SDS, 100mM $NaHCO_3$, 200mM NaCl) was
867 then added to IgG samples, H3K27Me3 samples, and inputs; decrosslinking reactions were allowed to
868 incubate overnight in a 65 degree Celsius water bath. Phenol-choloform DNA extraction was performed the
869 next day. Quantitative PCR was performed with 2x SYBR green mix (#RR420L, Takara Bio, Otsu, Shiga,
870 Japan) and primers against JAK1, STAT3, JAK2, PAX2, and beta actin (primers listed at the end of the
871 methods section). Signal was calculated from standard curves generated by serial dilution of an input sample,
872 and enrichment values were expressed as fold over input. RNA for RT-PCR was extracted with Trizol, and
873 concentration was determined by spectrometry. PCR reactions were run with primers against JAK1 and
874 GAPDH. cDNA synthesis was run on the MJ Mini Thermocycler from Bio-Rad, and PCR reactions were run on
875 the MJ Research DNA Engine Opticon 2 Continuous Fluorescence Detector using Opticon Monitor software.
876
877 **Immunofluorescence**
878
879 Whole brains were harvested on day 1 or 4 post-SE, bisected sagitally, fixed in 4% paraformaldehyde,
880 dehydrated in a series of graded TBS-Tween/ethanol solutions, embedded in paraffin, sectioned at 5μm and
881 subjected to immunofluorescence for NeuN, GFAP, total STAT3, and DAPI. Heat induced antigen retrieval was
882 performed in a 10mM citric acid buffer (pH 6.0). After a blocking step, mouse anti-NeuN (1:200 ab104224
883 Abcam, or 1:500 MAB377 from Millipore), rabbit anti-STAT3 (1:500 #12640 Cell Signaling), or rabbit anti-EZH2
884 (1:50 #5246 Cell Signaling) primary antibodies were applied and incubated overnight at 4°C. Slides were
885 washed with PBS then incubated with goat-anti-mouse or goat-anti-rabbit Alexa Fluor 488 (ab150113 Abcam
886 or A11005, A11008 from InVitrogen, respectively) and goat-anti-rabbit Alexa Fluor 594 (ab150080 Abcam or
887 Jackson ImmunoResearch) secondary antibodies at a concentration of 1:200 for one or two hours at room
888 temperature, followed in some experiments by two-hour incubation at room temperature with Alexa Fluro 488-
889 conjugated mouse anti-GFAP antibody (1:200) (#53-9892-82 Invitrogen). Nuclear DNA was stained with DAPI
890 (300 nM) or a DAPI-containing mounting media (#H-1200 Vector Laboratories, Burlingame, CA). Slides were
891 imaged at 20-40x magnification using a fluorescent microscope (Nikon E600 microscope with fluorescence or
892 Zeiss Axio Observer A1 epifluorescence microscope). Images were captured with Zeiss Axiovision or Cellsens
893 software (Olympus Life Science Solutions, Center Valley, PA). Image analysis and processing were performed
894 in ImageJ (NIH, https://imagej.nih.gov/ij/).
895
896 **Statistical analysis**
897
898 For all statistical analysis – with the exception of RNAseq data – FDR < 0.05 corrected for multiple
899 comparisons was considered statistically significant. Data were graphed as mean ± standard deviation (SD) in
900 Prism 9 software (Graphpad Software, La Jolla, CA). Statistical tests were also performed in Prism. Western
901 blot, seizure threshold, and spontaneous seizure data was analyzed by 2-way or 1-way ANOVA with the
902 Benjamini-Hochberg FDR method for multiple comparisons, or by unpaired t-test where appropriate.
903
904 Primer List
905 mouse-JAK1-Site1 (ChIP):
906 (forward) *CTCTGCTCGCTTTCCCGGAGATGC*
907 (reverse) *CTCGGAGGCTGGAGCGTGACTTCT*
908

909 mouse-JAK1-Site2 (ChIP):
910 (forward) *TGACTCGCACCCAGCCTGAAATGG*
911 (reverse) *GCGGCCCAGTCACCCGAAGAAATA*
912
913 mouse-JAK1-Site3 (ChIP):
914 (forward) *TTCGCGGGGCAAGGGAAAGGATTC*
915 (reverse) *CCACCGCTCAGGGCTCTGGGTTTT*
916
917 mouse-JAK2 (ChIP):
918 (forward) *CGCCGCTGCGGGATGTGAGTGC*
919 (reverse) *GGAGGCGGGATCGCAGGGAGAACC*
920
921 mouse-STAT3 (ChIP):
922 (forward) *CGGGCGAGCGCTGTACTTCCTA*
923 (reverse) *AAGCGAGCCGTATCAGGGCATTTA*
924
925 mouse-PAX2 (ChIP):
926 (forward) *GCGGCGCTCAGTCGCGTTCATAG*
927 (reverse) *CTCCCCGGAGTCTGGGCAGTCCA*
928
929 mouse-JAK1 (RT-PCR):
930 (forward) *GCGCCCAGCCTCGCTCGTC*
931 (reverse) *AACGCCATGGCATTGCAGTCCTCT*
932
933 mouse-GAPDH (RT-PCR):
934 (forward) *ACGGCAAATTCAACGGCACAGTCA*
935 (reverse) *TGGGGGCATCGGCAGAAGG*
936
937 **Funding.** Supported by CURE (AR), Lily's Fund (AR), NIH grant 1R01NS108756 (AR, RD) and
938 R01NS105628, R01NS102937, and R21NS120868 (JM).
939
940 **Acknowledgements.** We thank Asheebo Rojas for providing rat brain tissues in the DFP model.
941
942 **Conflict of Interest.** JM serves on the Scientific Advisory Board and has a Sponsored Research Agreement
943 with SAGE Therapeutics for work unrelated to this project. AR and RD have no conflicts of interest to declare.
944
945 References
946
947 1 Hirtz, D. *et al.* How common are the "common" neurologic disorders? *Neurology* **68**, 326 (2007).
948 https://doi.org/10.1212/01.wnl.0000252807.38124.a3
949 2 Gavvala, J. R. & Schuele, S. U. New-Onset Seizure in Adults and Adolescents: A Review. *Jama* **316**, 2657 (2016).
950 https://doi.org/10.1001/jama.2016.18625
951 3 Sankaraneni, R. & Lachhwani, D. Antiepileptic drugs--a review. *Pediatric Annals* **44**, e36 (2015).
952 https://doi.org/10.3928/00904481-20150203-10
953 4 Meyer, D. M. *et al.* Anti-inflammatory activity and neutrophil reductions mediated by the JAK1/JAK3 inhibitor,
954 CP-690,550, in rat adjuvant-induced arthritis. *Journal of Inflammation (London, England)* **7** (2010).
955 https://doi.org/10.1186/1476-9255-7-41
956 5 Dowty, M. E. *et al.* Preclinical to clinical translation of tofacitinib, a Janus kinase inhibitor, in rheumatoid
957 arthritis. *The Journal of Pharmacology and Experimental Therapeutics* **348**, 165 (2014).
958 https://doi.org/10.1124/jpet.113.209304
959 6 French, J. A. *et al.* Characteristics of medial temporal lobe epilepsy: I. Results of history and physical
960 examination. *Annals of Neurology* **34**, 774 (1993). https://doi.org/10.1002/ana.410340604
961 7 Trinka, E. *et al.* A definition and classification of status epilepticus--Report of the ILAE Task Force on
962 Classification of Status Epilepticus. *Epilepsia* **56**, 1515 (2015). https://doi.org/10.1111/epi.13121

963 8 Hesdorffer, D. C., Logroscino, G., Cascino, G., Annegers, J. F. & Hauser, W. A. Risk of unprovoked seizure after
964 acute symptomatic seizure: effect of status epilepticus. *Annals of Neurology* **44**, 908 (1998).
965 https://doi.org/10.1002/ana.410440609
966 9 Garriga-Canut, M. *et al.* 2-deoxy-D-glucose reduces epilepsy progression by NRSF-CtBP-dependent metabolic
967 regulation of chromatin structure. *Nature Neuroscience* **9**, 1382-1387 (2006). https://doi.org/10.1038/nn1791
968 10 Stafstrom, C. E., Roopra, A. & Sutula, T. P. Seizure suppression via glycolysis inhibition with 2-deoxy-D-glucose
969 (2DG). *Epilepsia* **49 Suppl 8**, 97 (2008). https://doi.org/10.1111/j.1528-1167.2008.01848.x
970 11 Stafstrom, C. E. *et al.* Anticonvulsant and antiepileptic actions of 2-deoxy-D-glucose in epilepsy models. *Annals of*
971 *Neurology* **65**, 435 (2009). https://doi.org/10.1002/ana.21603
972 12 Vezzani, A., Friedman, A. & Dingledine, R. J. The role of inflammation in epileptogenesis. *Neuropharmacology* **69**,
973 16 (2013). https://doi.org/10.1016/j.neuropharm.2012.04.004
974 13 Rojas, A. *et al.* A Novel Second-Generation EP2 Receptor Antagonist Reduces Neuroinflammation and Gliosis
975 After Status Epilepticus in Rats. *Neurotherapeutics: The Journal of the American Society for Experimental*
976 *NeuroTherapeutics* (2021). https://doi.org/10.1007/s13311-020-00969-5
977 14 Williams-Karnesky, R. L. *et al.* Epigenetic changes induced by adenosine augmentation therapy prevent
978 epileptogenesis. *Journal of Clinical Investigation* **123**, 3552-3563 (2013). https://doi.org/10.1172/jci65636
979 15 Liu, G. *et al.* Transient inhibition of TrkB kinase after status epilepticus prevents development of temporal lobe
980 epilepsy. *Neuron* **79**, 31 (2013). https://doi.org/10.1016/j.neuron.2013.04.027
981 16 Landis, S. C. *et al.* A call for transparent reporting to optimize the predictive value of preclinical research. *Nature*
982 **490**, 187 (2012). https://doi.org/10.1038/nature11556
983 17 Becker, A. J. *et al.* Correlated stage- and subfield-associated hippocampal gene expression patterns in
984 experimental and human temporal lobe epilepsy. *The European Journal of Neuroscience* **18**, 2792 (2003).
985 https://doi.org/10.1111/j.1460-9568.2003.02993.x
986 18 Borges, K., Shaw, R. & Dingledine, R. Gene expression changes after seizure preconditioning in the three major
987 hippocampal cell layers. *Neurobiology of Disease* **26**, 66 (2007). https://doi.org/10.1016/j.nbd.2006.12.001
988 19 Hansen, K. F., Sakamoto, K., Pelz, C., Impey, S. & Obrietan, K. Profiling status epilepticus-induced changes in
989 hippocampal RNA expression using high-throughput RNA sequencing. *Scientific Reports* **4** (2014).
990 https://doi.org/10.1038/srep06930
991 20 McClelland, S. *et al.* The transcription factor NRSF contributes to epileptogenesis by selective repression of a
992 subset of target genes. *eLife* **3** (2014). https://doi.org/10.7554/eLife.01267
993 21 Roopra, A. MAGIC: A tool for predicting transcription factors and cofactors driving gene sets using ENCODE data.
994 *PLoS computational biology* **16** (2020). https://doi.org/10.1371/journal.pcbi.1007800
995 22 Dingledine, R. *et al.* Transcriptional profile of hippocampal dentate granule cells in four rat epilepsy models.
996 *Scientific Data* **4** (2017). https://doi.org/10.1038/sdata.2017.61
997 23 Khan, N. *et al.* A systems approach identifies Enhancer of Zeste Homolog 2 (EZH2) as a protective factor in
998 epilepsy. *Plos One* **14** (2019). https://doi.org/10.1371/journal.pone.0226733
999 24 Pfisterer, U. *et al.* Identification of epilepsy-associated neuronal subtypes and gene expression underlying
1000 epileptogenesis. *Nature Communications* **11** (2020). https://doi.org/10.1038/s41467-020-18752-7
1001 25 Cid, E. *et al.* Sublayer- and cell-type-specific neurodegenerative transcriptional trajectories in hippocampal
1002 sclerosis. *Cell Reports* **35** (2021). https://doi.org/10.1016/j.celrep.2021.109229
1003 26 Kumar, P. *et al.* Single-cell transcriptomics and surface epitope detection in human brain epileptic lesions
1004 identifies pro-inflammatory signaling. *Nature Neuroscience* **25**, 956 (2022). https://doi.org/10.1038/s41593-022-
1005 01095-5
1006 27 Lund, I. V. *et al.* BDNF Selectively Regulates GABAA Receptor Transcription by Activation of the JAK/STAT
1007 Pathway. *Science Signaling* **1**, ra9 (2008). https://doi.org/10.1126/scisignal.1162396
1008 28 You, S. J., Jung, D. E., Kim, H. D., Lee, H. S. & Kang, H. C. Efficacy and prognosis of a short course of prednisolone
1009 therapy for pediatric epilepsy. *European journal of paediatric neurology: EJPN: official journal of the European*
1010 *Paediatric Neurology Society* **12**, 314 (2008). https://doi.org/10.1016/j.ejpn.2007.09.003
1011 29 Dubey, D. *et al.* Randomized Placebo-Controlled Trial of Intravenous Immunoglobulin in Autoimmune
1012 LGI1/CASPR2 Epilepsy. *Annals of Neurology* **87**, 313 (2020). https://doi.org/10.1002/ana.25655
1013 30 Gayatri, N. A., Ferrie, C. D. & Cross, H. Corticosteroids including ACTH for childhood epilepsy other than epileptic
1014 spasms. *The Cochrane Database of Systematic Reviews* (2007).
1015 https://doi.org/10.1002/14651858.CD005222.pub2

31 Lai, Y.-C. *et al.* Anakinra usage in febrile infection related epilepsy syndrome: an international cohort. *Annals of Clinical and Translational Neurology* **7**, 2467 (2020). https://doi.org/10.1002/acn3.51229

32 Grabenstatter, H. L. *et al.* The effect of STAT3 inhibition on status epilepticus and subsequent spontaneous seizures in the pilocarpine model of acquired epilepsy. *Neurobiology of Disease* **62**, 73 (2014). https://doi.org/10.1016/j.nbd.2013.09.003

33 Jiang, J. *et al.* Suppressing pro-inflammatory prostaglandin signaling attenuates excitotoxicity-associated neuronal inflammation and injury. *Neuropharmacology* **149**, 149 (2019). https://doi.org/10.1016/j.neuropharm.2019.02.011

34 Varvel, N. H. *et al.* Preclinical development of an EP2 antagonist for post-seizure cognitive deficits. *Neuropharmacology* **224** (2023). https://doi.org/10.1016/j.neuropharm.2022.109356

35 Rojas, A., Ganesh, T., Lelutiu, N., Gueorguieva, P. & Dingledine, R. Inhibition of the prostaglandin EP2 receptor is neuroprotective and accelerates functional recovery in a rat model of organophosphorus induced status epilepticus. *Neuropharmacology* **93**, 15 (2015). https://doi.org/10.1016/j.neuropharm.2015.01.017

36 Shen, X. *et al.* EZH1 mediates methylation on histone H3 lysine 27 and complements EZH2 in maintaining stem cell identity and executing pluripotency. *Molecular Cell* **32**, 491 (2008). https://doi.org/10.1016/j.molcel.2008.10.016

37 Zhu, Y. *et al.* Ablation of NF1 function in neurons induces abnormal development of cerebral cortex and reactive gliosis in the brain. *Genes & Development* **15**, 859 (2001). https://doi.org/10.1101/gad.862101

38 Basu, T. *et al.* Histone deacetylase inhibitors restore normal hippocampal synaptic plasticity and seizure threshold in a mouse model of Tuberous Sclerosis Complex. *Scientific Reports* **9** (2019). https://doi.org/10.1038/s41598-019-41744-7

39 Cilio, M. R. *et al.* Anticonvulsant action and long-term effects of gabapentin in the immature brain. *Neuropharmacology* **40**, 139 (2001). https://doi.org/10.1016/s0028-3908(00)00103-9

40 Bierkamper, G. G. & Cenedella, R. J. Induction of chronic epileptiform activity in the rat by an inhibitor of cholesterol synthesis, U18666A. *Brain Research* **150**, 343 (1978). https://doi.org/10.1016/0006-8993(78)90285-8

41 Liu, Z. & Holmes, G. L. Basic fibroblast growth factor is highly neuroprotective against seizure-induced long-term behavioural deficits. *Neuroscience* **76**, 1129 (1997). https://doi.org/10.1016/s0306-4522(96)00412-5

42 Applegate, C. D. & Tecott, L. H. Global increases in seizure susceptibility in mice lacking 5-HT2C receptors: a behavioral analysis. *Experimental Neurology* **154**, 522 (1998). https://doi.org/10.1006/exnr.1998.6901

43 Rho, J. M., Kim, D. W., Robbins, C. A., Anderson, G. D. & Schwartzkroin, P. A. Age-dependent differences in flurothyl seizure sensitivity in mice treated with a ketogenic diet. *Epilepsy Research* **37**, 233 (1999). https://doi.org/10.1016/s0920-1211(99)00068-6

44 Samoriski, G. M. & Applegate, C. D. Repeated generalized seizures induce time-dependent changes in the behavioral seizure response independent of continued seizure induction. *The Journal of Neuroscience: The Official Journal of the Society for Neuroscience* **17**, 5581 (1997).

45 Tipton, A. E. *et al.* Selective Neuronal Knockout of STAT3 Function Inhibits Epilepsy Progression, Improves Cognition, and Restores Dysregulated Gene Networks in a Temporal Lobe Epilepsy Model. *Annals of Neurology* (2023). https://doi.org/10.1002/ana.26644

46 Ahmed, M. M. *et al.* Altered Protein Profiles During Epileptogenesis in the Pilocarpine Mouse Model of Temporal Lobe Epilepsy. *Frontiers in Neurology* **12** (2021). https://doi.org/10.3389/fneur.2021.654606

47 Vishwakarma, S., Singh, S. & Singh, T. G. Pharmacological modulation of cytokines correlating neuroinflammatory cascades in epileptogenesis. *Molecular Biology Reports* **49**, 1437 (2022). https://doi.org/10.1007/s11033-021-06896-8

48 Martín-Suárez, S., Cortes, J. M. & Bonifazi, P. Blockage of STAT3 during epileptogenesis prevents GABAergic loss and imprinting of the epileptic state. *Brain: A Journal of Neurology* (2023). https://doi.org/10.1093/brain/awad055

49 Freeman, L. C. Centrality in social networks conceptual clarification. *Social Networks* **1**, 215-239 (1978).

50 Johnson, M. R. *et al.* Systems genetics identifies Sestrin 3 as a regulator of a proconvulsant gene network in human epileptic hippocampus. *Nature Communications* **6** (2015). https://doi.org/10.1038/ncomms7031

51 Kupferman, M. E. *et al.* Therapeutic suppression of constitutive and inducible JAK\STAT activation in head and neck squamous cell carcinoma. *Journal of Experimental Therapeutics & Oncology* **8**, 117 (2009).

1067 52 Hussain, S. F. *et al.* A Novel Small Molecule Inhibitor of Signal Transducers and Activators of Transcription 3
1068 Reverses Immune Tolerance in Malignant Glioma Patients. *Cancer Research* **67**, 9630 (2007).
1069 https://doi.org/10.1158/0008-5472.can-07-1243
1070 53 Iwamaru, A. *et al.* A novel inhibitor of the STAT3 pathway induces apoptosis in malignant glioma cells both in
1071 vitro and in vivo. *Oncogene* **26**, 2435 (2007). https://doi.org/10.1038/sj.onc.1210031
1072 54 Changelian, P. S. *et al.* Prevention of organ allograft rejection by a specific Janus kinase 3 inhibitor. *Science (New*
1073 *York, N.Y.)* **302**, 875 (2003). https://doi.org/10.1126/science.1087061
1074 55 *UCSC Genome Browser*, <https://genome.ucsc.edu/index.html> (2022).
1075 56 Konze, K. D. *et al.* An orally bioavailable chemical probe of the Lysine Methyltransferases EZH2 and EZH1. *ACS*
1076 *chemical biology* **8**, 1324 (2013). https://doi.org/10.1021/cb400133j
1077 57 Rocha, L. Subchronic treatment with antiepileptic drugs modifies pentylenetetrazol-induced seizures in mice: Its
1078 correlation with benzodiazepine receptor binding. *Neuropsychiatric Disease and Treatment* **4**, 619 (2008).
1079 https://doi.org/10.2147/ndt.s2118
1080 58 Baradaran Rahimi, V., Askari, V. R., Hosseini, M., Yousefsani, B. S. & Sadeghnia, H. R. Anticonvulsant Activity of
1081 Viola tricolor against Seizures Induced by Pentylenetetrazol and Maximal Electroshock in Mice. *Iranian Journal of*
1082 *Medical Sciences* **44**, 220 (2019).
1083 59 Cohen, S., Zwillich, S. H., Chow, V., Labadie, R. R. & Wilkinson, B. Co-administration of the JAK inhibitor CP-
1084 690,550 and methotrexate is well tolerated in patients with rheumatoid arthritis without need for dose
1085 adjustment. *British Journal of Clinical Pharmacology* **69**, 143 (2010). https://doi.org/10.1111/j.1365-
1086 2125.2009.03570.x
1087 60 Maguire, J. Epileptogenesis: More Than Just the Latent Period. *Epilepsy Currents* **16**, 31 (2016).
1088 https://doi.org/10.5698/1535-7597-16.1.31
1089 61 Stapels, M. *et al.* Polycomb Group Proteins as Epigenetic Mediators of Neuroprotection in Ischemic Tolerance.
1090 *Science Signaling* **3**, ra15 (2010). https://doi.org/10.1126/scisignal.2000502
1091 62 Jenkins, A., Franks, N. P. & Lieb, W. R. Effects of temperature and volatile anesthetics on GABA(A) receptors.
1092 *Anesthesiology* **90**, 484 (1999). https://doi.org/10.1097/00000542-199902000-00024
1093 63 Brosnan, R. J. & Thiesen, R. Increased NMDA receptor inhibition at an increased Sevoflurane MAC. *BMC*
1094 *anesthesiology* **12** (2012). https://doi.org/10.1186/1471-2253-12-9
1095 64 Xue, H. *et al.* Sevoflurane post-conditioning alleviates neonatal rat hypoxic-ischemic cerebral injury via Ezh2-
1096 regulated autophagy. *Drug Design, Development and Therapy* **13**, 1691 (2019).
1097 https://doi.org/10.2147/dddt.s197325
1098 65 Choi, J.-S. *et al.* Upregulation of gp130 and differential activation of STAT and p42/44 MAPK in the rat
1099 hippocampus following kainic acid-induced seizures. *Molecular Brain Research* **119**, 10 (2003).
1100 https://doi.org/10.1016/j.molbrainres.2003.08.010
1101 66 Wang, H. *et al.* LncRNA-UCA1 inhibits the astrocyte activation in the temporal lobe epilepsy via regulating the
1102 JAK/STAT signaling pathway. *Journal of Cellular Biochemistry* **121**, 4261 (2020).
1103 https://doi.org/10.1002/jcb.29634
1104 67 Iori, V., Frigerio, F. & Vezzani, A. Modulation of neuronal excitability by immune mediators in epilepsy. *Current*
1105 *Opinion in Pharmacology* **26**, 118 (2016). https://doi.org/10.1016/j.coph.2015.11.002
1106 68 Reetz, O., Stadler, K. & Strauss, U. Protein kinase C activation mediates interferon-β-induced neuronal
1107 excitability changes in neocortical pyramidal neurons. *Journal of Neuroinflammation* **11** (2014).
1108 https://doi.org/10.1186/s12974-014-0185-4
1109 69 Danis, E. *et al.* Ezh2 Controls an Early Hematopoietic Program and Growth and Survival Signaling in Early T Cell
1110 Precursor Acute Lymphoblastic Leukemia. *Cell Reports* **14**, 1953 (2016).
1111 https://doi.org/10.1016/j.celrep.2016.01.064
1112 70 Wee, Z. N. *et al.* EZH2-mediated inactivation of IFN-γ-JAK-STAT1 signaling is an effective therapeutic target in
1113 MYC-driven prostate cancer. *Cell Reports* **8**, 204 (2014). https://doi.org/10.1016/j.celrep.2014.05.045
1114 71 Kim, E. *et al.* Phosphorylation of EZH2 activates STAT3 signaling via STAT3 methylation and promotes
1115 tumorigenicity of glioblastoma stem-like cells. *Cancer Cell* **23**, 839 (2013).
1116 https://doi.org/10.1016/j.ccr.2013.04.008
1117 72 Dasgupta, M., Dermawan, J. K. T., Willard, B. & Stark, G. R. STAT3-driven transcription depends upon the
1118 dimethylation of K49 by EZH2. *Proceedings of the National Academy of Sciences of the United States of America*
1119 **112**, 3985 (2015). https://doi.org/10.1073/pnas.1503152112

1120 73 Cha, T.-L. *et al.* Akt-mediated phosphorylation of EZH2 suppresses methylation of lysine 27 in histone H3.
1121 *Science (New York, N.Y.)* **310**, 306 (2005). https://doi.org/10.1126/science.1118947
1122 74 Yan, J. *et al.* EZH2 phosphorylation by JAK3 mediates a switch to noncanonical function in natural killer/T-cell
1123 lymphoma. *Blood* **128**, 948 (2016). https://doi.org/10.1182/blood-2016-01-690701
1124 75 Love, M. I., Huber, W. & Anders, S. Moderated estimation of fold change and dispersion for RNA-seq data with
1125 DESeq2. *Genome Biology* **15** (2014). https://doi.org/10.1186/s13059-014-0550-8
1126 76 Wolf, F. A., Angerer, P. & Theis, F. J. SCANPY: large-scale single-cell gene expression data analysis. *Genome*
1127 *Biology* **19** (2018). https://doi.org/10.1186/s13059-017-1382-0
1128 77 Assenov, Y., Ramírez, F., Schelhorn, S.-E., Lengauer, T. & Albrecht, M. Computing topological parameters of
1129 biological networks. *Bioinformatics (Oxford, England)* **24**, 282 (2008).
1130 https://doi.org/10.1093/bioinformatics/btm554
1131 78 Pedregosa, F. *et al.* Scikit-learn: Machine Learning in Python. *Journal of Machine Learning Research* **12**, 2825
1132 (2011).
1133 79 Madisen, L. *et al.* A robust and high-throughput Cre reporting and characterization system for the whole mouse
1134 brain. *Nature Neuroscience* **13**, 133 (2010). https://doi.org/10.1038/nn.2467
1135 80 Racine, R. J. Modification of seizure activity by electrical stimulation. II. Motor seizure. *Electroencephalography*
1136 *and Clinical Neurophysiology* **32**, 281 (1972). https://doi.org/10.1016/0013-4694(72)90177-0
1137 81 Basu, T. *et al.* Hypothalamic-pituitary-adrenal axis dysfunction worsens epilepsy outcomes and increases SUDEP
1138 risk. (Neuroscience, 2022).
1139
1140
1141
1142

SUPPLEMENTAL FIGURES

S1. Synapsin1-Cre expression and recombination occur in neurons, and conditional knockout diminishes EZH2 induction post-SE.

S2. Neuronal ablation of EZH2 does not alter latency to 1st Class V seizure during kainate injections.

S3. Ontology networks for the mouse-Black and human-Brown clusters.

S4. Transient induction of STAT3 in wildtype animals is observed across models of SE.

S5. Other STAT family proteins are hyper-induced in EZH2nKO mice.

S6. Western blot quantifications in shNT and shEZH2 N2A cells.

S7. JAK2 activity is not required for hyper-activation of STAT3 in the absence of EZH2.

S8. Western blot quantifications in N2A cells transfected with control plasmids or overexpressing JAK1.

S9. H3K27Me3 ChIP-PCR at JAK1 (Sites 1 and 3), JAK2, and STAT3.

S10. CP treatment window selection and target engagement.

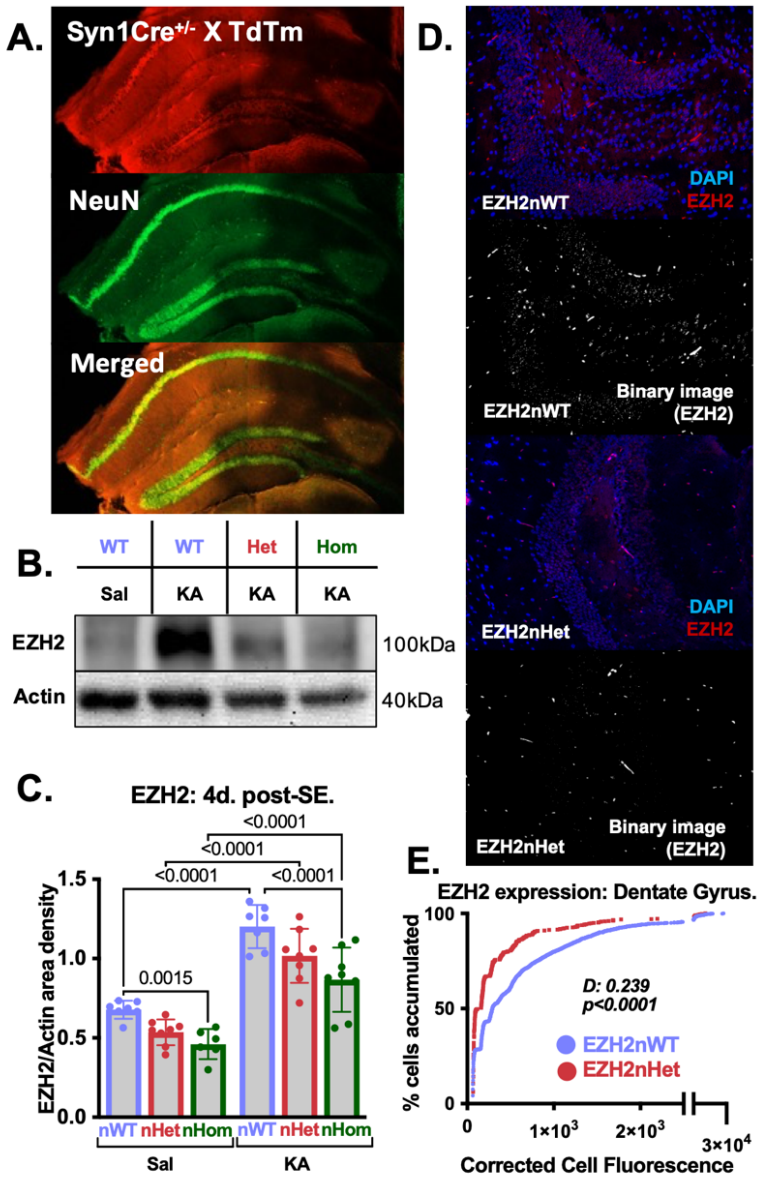

Fig. S1. Synapsin1-Cre expression and recombination occur in neurons, and conditional knockout diminishes EZH2 induction post-SE. **(A)** Syn1Cre$^{+/-}$ driver mice were bred with TdTm reporter mice. Immunofluorescence was performed on hippocampal sections, probing with the neuronal marker NeuN. TdTm colocalizes with NeuN. **(B)** Representative western blot probed for EZH2 in EZH2nWT, EZH2nHet, and EZH2nHom mice. **(C)** Quantification of western blot in panel B (2-way ANOVA; n=5-7). **(D)** (Left) Merged immunofluorescence images of the dentate gyrus labeling DAPI (blue), EZH2 (red), and (right) EZH2 binary images generated after auto-thresholding. Images were captured at 20x magnification in KA-injected EZH2nWT and EZH2nHet mice 4 days post-SE (n=1). **(E)** Quantification of binary images in panel D as a cumulative frequency distribution (Kolmogorov-Smirvnov test; D:0.239, $p<10^{-4}$).

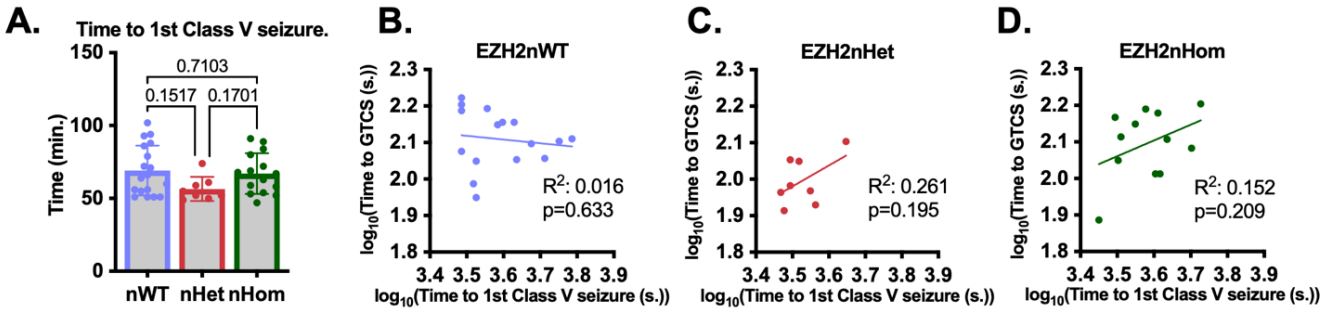

Fig. S2. Neuronal ablation of EZH2 does not alter latency to 1st Class V seizure during kainate injections. **(A)** Deletion of one or both EZH2 alleles does not alter time to first class V seizure during induction of SE with kainate (1-way ANOVA; n=8-18). **(B-D)** There is no correlation between time to first class V seizure and time to generalized tonic clonic seizure post-SE during fluorothyl testing (Pearson correlation; **nWT**: R^2:0.016, p=0.633, **nHet**: R^2:0.261, p=0.195, **nHom**: R^2:0.152, p=0.209; n=8-15).

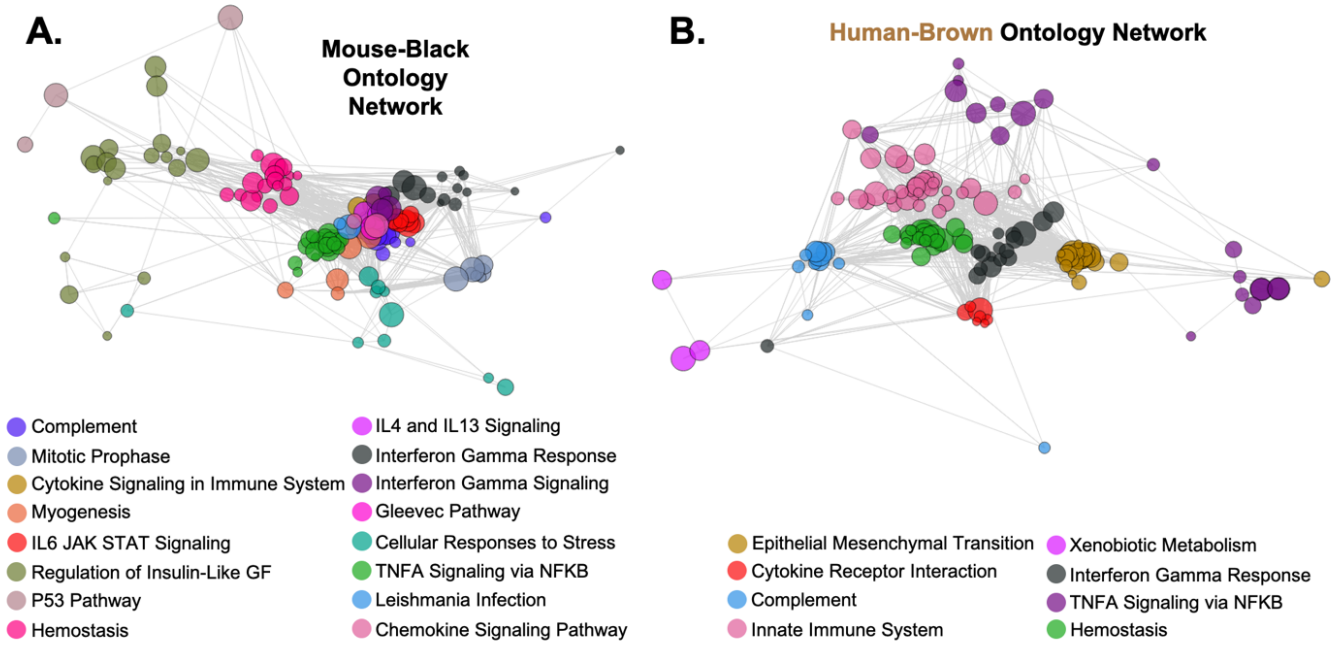

Fig. S3. Ontology networks for the mouse-Black and human-Brown clusters. **(A)** The 439 mouse-Black cluster genes and **(B)** 850 human-Brown cluster genes were compared to gene lists associated with terms in KEGG, Reactome, Biocarta, and Hallmark databases; terms with an odds ratio>1 and p<0.05 across all databases were sorted into ten communities via a network approach. Community names are the ontological term with the highest odds ratio in the community.

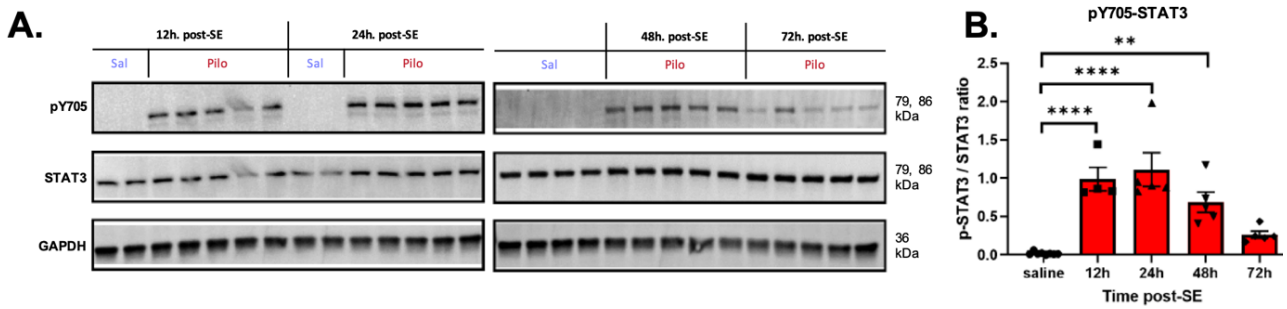

Fig S4. Transient induction of STAT3 in wildtype animals is observed across models of SE. **(A)** Hippocampi were collected from wildtype control and pilo-SE rats at 12, 24, 48, and 72h. post-SE and protein lysates were run on western blots for pY705-STAT3, total STAT3, and GAPDH. **(B)** pY705-STAT3 is robustly induced up to 48h. post-SE, but begins to diminish by 72h. post-SE (1-way ANOVA; n=4-8).

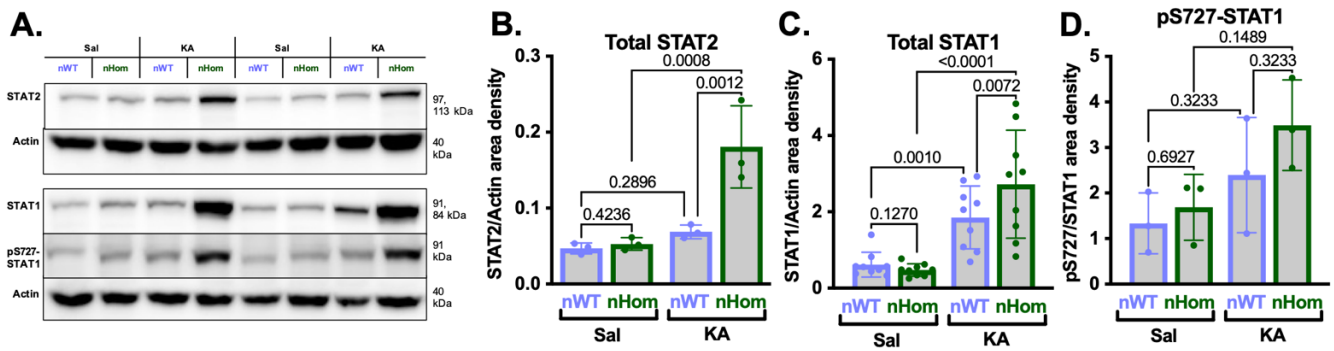

Fig S5. Other STAT family proteins are hyper-induced in EZH2nKO mice. **(A)** Representative western blots for total STAT2, total STAT1, phospho-STAT1 (S727) and beta-actin on day 4 post-SE. For all proteins quantified in panels B-D, deletion of an EZH2 allele in naïve animals does not alter protein levels. **(B)** Total STAT2 is robustly induced after SE in EZH2nHom mice only by 3.4-fold (p=0.0008), 2.6-fold greater than EZH2nWT mice post-SE (p=0.001) (2-way ANOVA; n=3). **(C)** Total STAT1 protein is induced by 3-fold (p=0.001) in EZH2nWT mice post-SE, and 5.7-fold ($p<10^{-4}$) in EZH2nHom mice post-SE. Total STAT1 is hyper-induced in EZH2nHom mice following seizures by 1.5-fold (p=0.007) compared to EZH2nWT mice (2-way ANOVA; n=9). **(D)** pS727-STAT1 is not robustly altered across the four conditions, but trends toward a 2-fold (p=0.148) induction in EZH2nHom mice post-SE (2-way ANOVA; n=3).

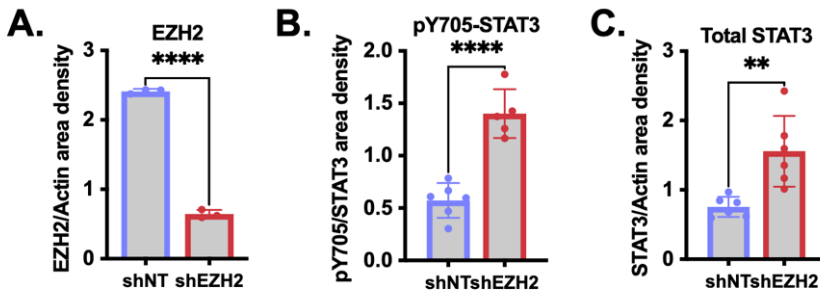

Fig. S6. Western blot quantifications in shNT and shEZH2 N2A cells. **(A)** Protein was harvested from shNT and shEZH2 cells for western blot analysis. A 3.7-fold reduction in EZH2 protein in the knockdown cells was confirmed by western blot **(A)** (unpaired t-test; $p<10^{-4}$; n=3). We observe a 2.4-fold induction of pY705-STAT3 **(B)** in shEZH2 cells (unpaired t-test; $p<10^{-4}$; n=5-6). **(C)** Total STAT3 protein was induced by 2.1-fold in shEZH2 cells (unpaired t-test; p=0.004; n=6).

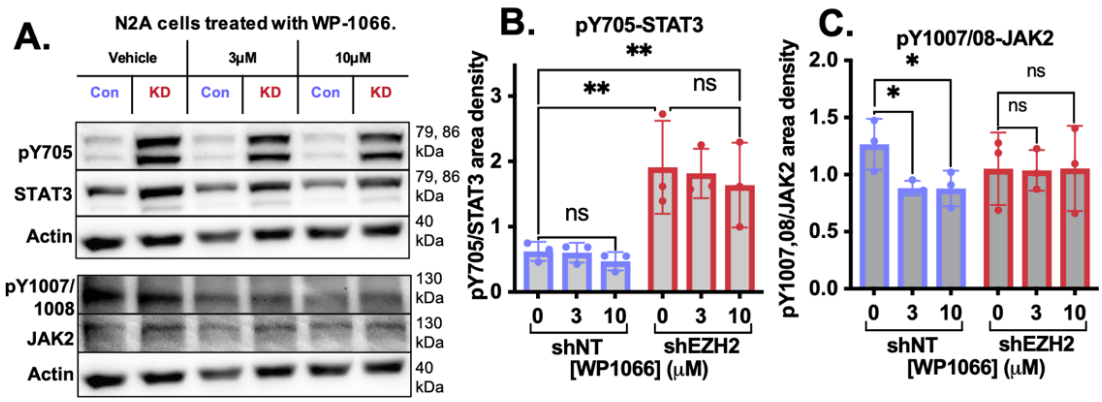

Fig. S7. JAK2 activity is not required for hyper-activation of STAT3 in the absence of EZH2. **(A)** shNT and shEZH2 cells were treated with the JAK2/STAT3 inhibitor WP1066 to a final concentration of 0 (DMSO), 3, or 10μM for one hour. Protein was harvested and subjected to western blot analysis. **(B)** Quantification of western blots in panel A. pY705-STAT3 is induced in vehicle-treated shEZH2 cells by 3-fold (p=0.005). WP1066 does not alter pY705 levels in control or knockdown cells at any concentration (2-way ANOVA; n=3). **(C)** WP1066 reduces pY1007/08-JAK2 in shNT cells by 1.4-fold for both concentrations (p=0.014), but no change was observed in knockdown cells (2-way ANOVA; n=3).

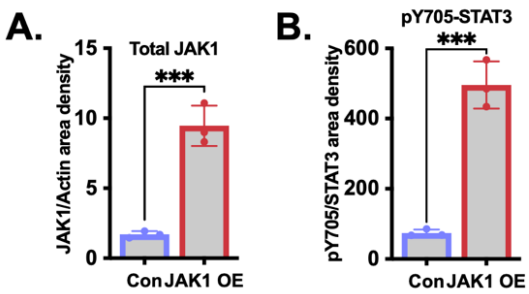

Fig. S8. Western blot quantifications in N2A cells transfected with control plasmids or overexpressing JAK1. N2A cells were transfected with either Adtrack plasmid (Con) or FLAG-JAK1 (JAK1 OE), and samples were subjected to western blotting. **(A)** A 5.5-fold induction of JAK1 upon overexpression was confirmed (unpaired t-test; p=0.0008; n=3). **(B)** pY705-STAT3 levels were induced by 6.7-fold in JAK1 OE cells (p=0.0004) in the absence of changes to total STAT3 (unpaired t-test; p=0.0004; n=3).

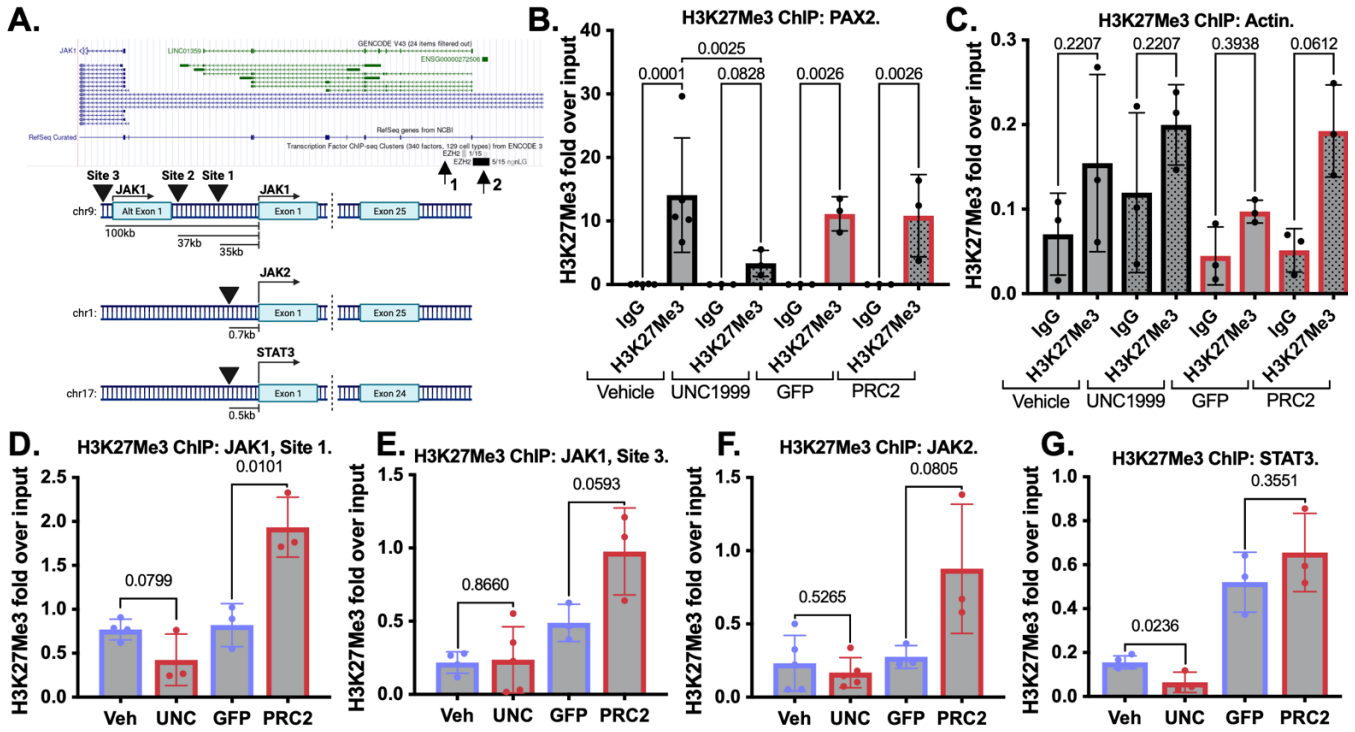

Fig. S9. H3K27Me3 ChIP-PCR at JAK1 (Sites 1 and 3), JAK2, and STAT3. **(A)** Image from the UCSC Genome Browser depicting putative EZH2 binding sites 1 and 2 on JAK1. Schematics representing all EZH2 binding sites on JAK1, JAK2, and STAT3. **(B)** Positive control PAX2. H3K27Me3 is enriched in both vehicle-treated ($p=10^{-4}$) and GFP-transfected ($p=0.008$) N2A cells. Treatment with 10mM UNC1999 reduces H3K27Me3 enrichment ($p=0.004$), and overexpression of PRC2 increases H3K27Me3 enrichment ($p=0.009$) (1-way ANOVA; n=3-5). **(C)** Negative control Actin. H3K27Me3 is not enriched unless PRC2 is overexpressed ($p=0.0116$) (1-way ANOVA; n=3). **(D-G)** Parallel ChIP-qPCR experiments performed with antibodies against H3K27Me3, wherein N2A cells were treated with either vehicle or 10mM UNC1999 for 24 hours, or transfected with expression vectors for GFP-EZH2, SUZ12, and EED or GFP. qPCR was performed. Results were graphed as fold H3K27Me3 over input. At JAK1, Site 1 **(D)**, treatment with 10mM UNC1999 leads to a trends towards reduced H3K27Me3 enrichment ($p=0.079$), and overexpression of PRC2 increases H3K27Me3 enrichment ($p=0.010$) (unpaired t-test; n=3-4). At JAK1, Site 3 **(E)**, treatment with 10mM UNC1999 does not alter H3K27Me3 enrichment, and overexpression of PRC2 leads to a trend towards increased H3K27Me3 enrichment ($p=0.059$) (unpaired t-test; n=3-4). At JAK2 **(F)**, treatment with 10mM UNC1999 does not alter H3K27Me3 enrichment, and overexpression of PRC2 leads to a trend towards increased H3K27Me3 enrichment ($p=0.080$) (unpaired t-test; n=3-4). At STAT3 **(G)**, treatment with 10mM UNC1999 reduces H3K27Me3 enrichment ($p=0.023$), but overexpression of PRC2 does not alter H3K27Me3 enrichment (unpaired t-test; n=3-4).

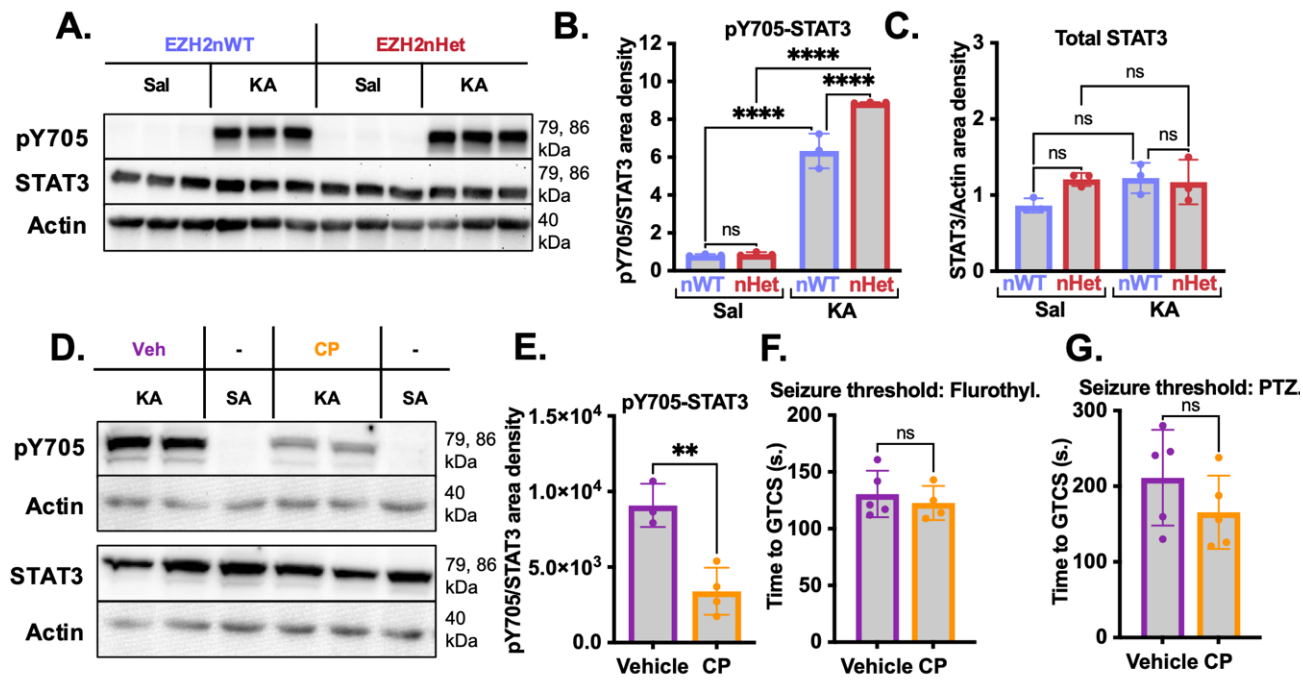

Fig. S10. CP treatment window selection and target engagement. **(A-C)** Hippocampi from saline- or kainate-injected EZH2nWT and EZH2nHet mice were harvested on day 1 post-SE to quantify pY705-STAT3 induction. **(B)** All kainate animals exhibit robust induction of pY705 on day 1 post-SE ($p<10^{-4}$), with EZH2nHet mice showing a 1.4-fold greater induction of pY705 over EZH2nWT mice ($p<10^{-4}$) (2-way ANOVA; n=3). **(C)** Total STAT3 is not altered by EZH2 deletion or kainate injection (2-way ANOVA; n=3). **(D)** After induction of SE and CP treatment at 6, 12, and 24h. post-SE, a cohort of mice was sacrificed 3 hours after the last injection, and hippocampi were extracted to confirm drug target engagement via western blot. **(E)** Protein extracts from treated and untreated animals were run alongside extracts from naïve mice (lanes 1,4) to confirm the pY705 induction typically observed on day 1 post-SE. Drug-treated animals exhibited a 2.7-fold reduction in pY705 compared to vehicle-treated animals (unpaired t-test; p=0.004; n=3). **(F-G)** Naïve wildtype mice were pre-treated with CP690550 or vehicle (i.p., 15mg/kg) 30 minutes prior to threshold testing with flurothyl or PTZ (i.p., 45mg/kg). Time to generalized tonic clonic seizure was recorded. Results were analyzed by unpaired t-test. CP690550 pre-treatment does not alter **(F)** flurothyl (unpaired t-test; p=0.544; n=4-5) or **(G)** PTZ seizure threshold (unpaired t-test; p=0.236; n=5).